

Tm³⁺:ZBLAN Fiber Lasers and their Applications for Spectroscopy

By Kishor Ramaswamy



Department of Electrical & Computer Engineering

McGill University

Montreal, Quebec, Canada

August 2014

A thesis submitted to McGill University in partial fulfillment of the requirements for the degree of Master of Engineering.

©Copyright 2014 Kishor Ramaswamy

ACKNOWLEDGEMENTS

I would like to thank first and foremost my supervisor Professor Lawrence Chen for providing me with the opportunity to complete my Master's degree. His constant help and support through these two years were essential to the successful completion of my degree, and I am extremely grateful. He provided research ideas and help with experimental difficulties, as well as motivation when it came time to writing. I would also like to thank my colleague Chenglai Jia with whom I worked very closely through my degree. We began our respective degrees at the same time shared ideas, helped each other with experiments and provided support for each other. I would also like to thank my colleagues Thibault North and Sandrine Fillion-Côté for their help and motivation throughout my degree.

Outside of Photonics, I was fortunate to have a few very close friends from McGill who inspired and helped me in their own way. My gratitude goes out to George Xereas and Stefanos Koskinas for always being there for me, through the good and bad times. They provided a constant sounding board for my ideas and problems, and were always there to help in any way that they good. I would also like to thank Emmanuella Lambropoulos for her motivation, support and inspiration, and always pushing me to do the best I possibly could. I definitely would not have made it through these two years without the help of all these individuals.

I would lastly like to thank my parents and my brother for their unconditional love and support. They provided a wealth of knowledge and experience, having gone through graduate degrees themselves.

ABSTRACT

Thulium ions (Tm^{3+}) provide an effective means for developing fiber lasers at a wide range of wavelengths. Additionally, the extended transmission window of ZBLAN glass allows for operation well into the mid-infrared range. This thesis presents the design of several single and multi-wavelength Tm^{3+} :ZBLAN fiber lasers.

First, an optimized laser cavity operating around 1480 nm is designed by measuring several different cavity configurations and lengths of gain fiber. Using a 34 cm length of gain fiber and a 4% Fresnel air reflection as the output mirror/coupler, 32% conversion efficiency is obtained, with a threshold pump power of 400 mW and a maximum output power around 400 mW.

Next, a dual-band Tm^{3+} :ZBLAN fiber laser is designed, emitting simultaneously around 810 nm through the ${}^3\text{H}_4 \rightarrow {}^3\text{H}_6$ transition and around 1480 nm through the ${}^3\text{H}_4 \rightarrow {}^3\text{F}_4$ transition. This is the first demonstration of a fiber laser which uses the same piece of gain fiber for two different transitions which share the same upper energy level (${}^3\text{H}_4$ in this case). Simultaneous emission at both laser wavelengths with 20% slope efficiencies is obtained.

Finally, a three-wavelength Tm^{3+} :ZBLAN fiber laser emitting at 1460/1503/1873 nm is designed using two independent gain branches. Simultaneous operation at all three wavelengths is obtained, with approximately 10 mW output power at each wavelength. The peak fluctuations are stable within 1.5 dB. Wavelength switching through a polarization controller is also demonstrated in the 1460/1503 laser branch. The laser was then used in single-pass absorption measurements for detecting water in acetone. Molar absorptivities within 10-20% of the theoretical values are obtained from the absorption measured at each individual wavelength.

SOMMAIRE

Les ions de Thulium (Tm^{3+}) fournissent une manière effective pour développer des lasers à fibre émettant une large gamme de longueurs d'ondes. De plus, utiliser le verre ZBLAN permet d'opérer dans la région infrarouge à l'aide d'une transmission prolongée. Cette thèse présente la conception de plusieurs lasers à fibres de type Tm^{3+} :ZBLAN, émettant à une ou plusieurs longueurs d'ondes.

Premièrement, une cavité de laser optimisée, émettant autour de 1480 nm est construite en mesurant des configurations de cavités et longueur de fibre de gain différent. Avec une longueur de 34 cm et en utilisant une réflexion de l'air Fresnel de 4% pour le miroir de sortie, 32% d'efficacité est obtenue, avec un seuil de 400 mW de puissance de pompe et une puissance de laser maximale de 400 mW.

Ensuite, un laser à fibre de type Tm^{3+} :ZBLAN à deux bandes est construit, émettant simultanément autour de 810 nm avec la transition ${}^3H_4 \rightarrow {}^3H_6$ et autour de 1480 nm avec la transition ${}^3H_4 \rightarrow {}^3F_4$. Il s'agit de la première démonstration d'un laser à fibre qui utilise la même fibre de gain pour deux transitions différentes qui partagent le même niveau d'énergie supérieur (en ce cas, 3H_4). Une émission simultanée à ces deux longueurs d'ondes de laser avec 20% d'efficacité est obtenue.

Finalement, un laser à fibre de type Tm^{3+} :ZBLAN à trois longueurs d'ondes émettant à 1460/1503/1873 nm est construit avec deux branches de gain indépendantes. Une émission simultanée à ces trois longueurs d'ondes est obtenue, avec 10 mW de puissance à chaque longueur d'onde. Les fluctuations de puissance sont stables à l'intérieur de 1.5 dB. Le laser est ensuite utilisé dans une mesure d'absorption 'single-pass' pour détecter l'eau dans l'acétone. Les absorptivités molaires calculées sont de 10-20% des valeurs théoriques avec les mesures obtenues de chaque longueur d'onde.

Table of Contents

Chapter 1 Introduction	1
1.1 History of Fiber Lasers.....	1
1.2 Advantages and Applications of Fiber Lasers	2
1.3 Need for Fluoride Fiber	3
1.4 Motivation for Mid-IR Sources.....	7
1.5 Thesis Objectives and Achievements.....	9
1.6 Publications.....	10
1.7 Outline of Thesis	11
Chapter 2 Background	12
2.1 Rare-Earth Elements	12
2.1.1 Introduction	12
2.1.2 Thulium	13
2.3 Review of multi-wavelength Tm^{3+} :ZBLAN Fiber Lasers.....	21
2.3 Summary	25
Chapter 3 Lasing at 1480 nm	26
3.1 Introduction	26
3.2 Experimental Setup.....	29
3.3 Experimental Results	31
3.4 Conclusion.....	36
Chapter 4 Dual-Band Lasing at 810/1480 nm.....	38
4.1 Introduction	38
4.2 Experimental Setup.....	39
4.3 Experimental Results	42
4.4 Conclusion.....	47
Chapter 5 Triple-Wavelength Laser at 1460/1503/1873 nm.....	49
5.1 Introduction	49
5.2 Experimental Setup.....	51
5.2.1 Three-Wavelength Fiber Laser.....	51
5.2.2 Absorption Measurements	53
5.3 Experimental Results	54

5.3.1 Three-Wavelength Laser Characterization	54
5.3.2 Water in Acetone Absorption Measurements.....	59
5.4 Conclusion.....	60
Chapter 6 Conclusion and Future Work	62
Appendix A.....	65

List of Tables

Table 3.1: Threshold and slope efficiency for different lengths using optimum high conversion efficiency configuration.....	34
Table 3.1: Summary of conversion efficiency for all six configurations using six different lengths of ZBLAN gain fiber.....	36
Table 3.2: Summary of threshold power for all six configurations using six different lengths of ZBLAN gain fiber.....	36
Table 5.1: Molar Absorptivity coefficients in [$\text{L mol}^{-1} \text{m}^{-1}$] obtained from the single-pass absorption measurements vs. theoretical values.....	60

List of Figures

Figure 1.1: Schematic describing the different components of a laser [1].....	1
Figure 1.2: Loss profile of silica fiber [5]	4
Figure 1.3: Attenuation profile of ZBLAN fiber provided by IRphotonics [8].....	6
Figure 1.4: Absorption profiles of typical chemicals [12]	8
Figure 2.1: Electronic transitions of Tm^{3+} ions [6]	14
Figure 2.2: Three-level laser example showing fast and slow transitions	15
Figure 2.3: Comparison of output power vs. incident power for a Tm^{3+} :silica fiber laser (square) and a Tm^{3+} :ZBLAN fiber laser (circle) operating at 1900 nm [18]	17
Figure 2.4: Up-conversion pumping at 1064 nm in Tm^{3+} ions	18
Figure 2.5: Output power vs. pump power for a 2300 nm Tm^{3+} :ZBLAN fiber laser [21] ..	19
Figure 2.6: Experimental (dotted) and simulated (solid) output power vs. pump power curves for a 1480 nm Tm^{3+} :ZBLAN fiber laser [22].....	19
Figure 2.7: Output power vs. pump power for a 810 nm Tm^{3+} :ZBLAN fiber laser [24]	20
Figure 2.8: Transition diagram for dual-wavelength emission at 785 nm and 810 nm [27]	22
Figure 2.9: Multi-wavelength spectrum around 785 and 810 nm [28]	22
Figure 2.10: Dual-wavelength Tm^{3+} :ZBLAN fiber laser operating around 800 nm [30] ..	24
Figure 2.11: Dual-wavelength Tm^{3+} :ZBLAN fiber laser operating around 1480 nm [31]..	24
Figure 3.1: Upconversion pumping at 1064 nm to produce 1480 nm lasing	27
Figure 3.2: Dual-wavelength up-conversion pump configurations at a) 1064/1560 nm b) 1047/1410 nm c) 1050/800 nm d) 1410/1560 nm	29
Figure 3.3: Laser cavity with a loop mirror a) Pumping through the WDM coupler b) Pumping through the FBG	30
Figure 3.4: Low-loss laser cavity a) Pumping through the WDM coupler b) Pumping through the FBG.....	30
Figure 3.5: Output power for each configuration using a 34cm piece of ZBLAN fiber	33
Figure 3.6: Output power vs. Input power curves for different lengths using high conversion efficiency configuration.....	34
Figure 3.7: Spectrum of lasing at 1480 nm, using a 34 cm length of ZBLAN fiber.....	35
Figure 4.1: Upconversion pumping at 1064 nm to produce dual-band lasing at 810 nm and 1480 nm	39
Figure 4.2: Dual-band fiber laser cavity. Dashed boxes represent that a measurement was done with and without the component.	40
Figure 4.3: Pigtailed placed on XYZ translation stages.....	41
Figure 4.4: Output Power vs. Pump power without a PC for a 52cm Length of Gain Fiber	44
Figure 4.5: Output Power vs. Pump Power without a PC for a 140 cm Length of Gain Fiber	44
Figure 4.6: Output Power vs. Pump Power with a PC for a 60 cm Length of Gain Fiber ..	45

Figure 4.7: Output Power vs. Pump Power with a PC for an 85 cm Length of Gain Fiber	46
Figure 4.8: Output spectrum of dual-band fiber laser	47
Figure 5.1: Near-Infrared Region Absorption Spectrum of Water [41]	50
Figure 5.2: Tm ³⁺ :ZBLAN three-wavelength fiber laser configuration.....	52
Figure 5.3: Experimental setup using three-wavelength laser for absorption measurements	53
Figure 5.4: Output power at λ_1 and λ_2 vs. P_{1064} , with P_{1560} on and off	56
Figure 5.5: Output power at λ_3 vs. P_{1560} with P_{1064} on and off.....	56
Figure 5.6: Output spectrum of the three-wavelength laser operation for $P_{1064} \sim 1500$ mW and $P_{1560} \sim 500$ mW	57
Figure 5.7: Output power fluctuations of three-wavelength laser with $P_{1064} = 1500$ mW and $P_{1560} = 500$ mW.....	58
Figure 5.8: Output spectrum showing switching between (a) single-wavelength at λ_2 (b) single-wavelength at λ_1 (c) dual-wavelength at λ_1/λ_2 nm.....	59
Figure 5.9: Absorption of water in acetone at (a) 1460 nm (b) 1503 nm (c) 1873 nm.....	60

Chapter 1 Introduction

1.1 History of Fiber Lasers

A laser is a coherent light source that consists of a gain medium, an external energy source and a cavity, as shown in Fig. 1.1. The word was originally an acronym for light amplification by stimulated emission of radiation. It has an almost fully reflective surface on one end, and a partially reflecting surface – which also serves as the output – on the other end.

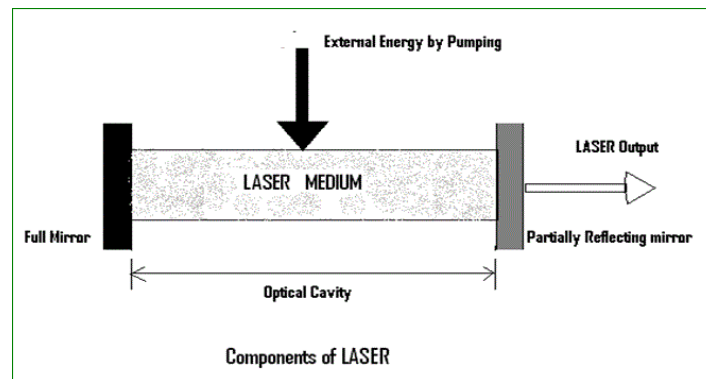


Figure 1.1: Schematic describing the different components of a laser [1]

A fiber laser is one where the gain medium is typically a rare-earth doped optical fiber. The rare-earth element can be one of Neodymium (Nd), Erbium (Er), Ytterbium (Yb), Thulium (Tm), Holmium (Ho), Cerium (Ce) or many others. The external energy source, defined as the pump, is another light source which is used to excite electrons in the doped-fiber to a higher energy state, enabling the release of photons as the electrons return to a lower energy state. The cavity is most commonly formed on one end by an almost fully reflective (> 99%) fiber Bragg grating (FBG), which is a wavelength-specific reflector created through periodic variations in the refractive index of the fiber core. The other end of the cavity is formed by a partially reflective surface, with reflectivity's ranging

from very low (4% air reflection) to very high (99% reflective FBG). The transmission through this partially reflective surface is used as the laser output.

The first fiber laser was demonstrated in 1961 by Elias Snitzer *et al.* from American Optical, a company that was moving into electro-optics [2]. It consisted of a Neodymium-doped fiber, pumped by a flash lamp, emitting at 1060 nm. Progress was slow following this demonstration, and there was little interest for the next 20-25 years due to the lack of high-efficiency pump sources and low-loss fibers. However, since the demonstration of a Neodymium-doped silica fiber laser in 1985 [3], research into all types of rare-earth doped fiber lasers has taken off.

1.2 Advantages and Applications of Fiber Lasers

Modern day fiber lasers have uses in almost all fields, both industrial and scientific. They are widely used in telecommunications, primarily for amplification. Erbium doped fiber amplifiers (EDFA) and Raman amplifiers both rely heavily on fiber lasers and have been two of its main proponents. Fiber lasers are also used for cutting and drilling purposes, replacing solid-state lasers and other mechanical tools. Furthermore, they are used in fields such as biomedical sensing, spectroscopy and chemical detection, as well as in military applications such as light detection and ranging (LIDAR) and missile defense.

Fiber lasers are very widely used because the advantages that they provide are numerous. Optical fibers offer very high heat dissipation, enabling them to create extremely high-powered lasers without being damaged. Indeed, a 600 W Neodymium-doped fiber laser has recently been demonstrated by Southampton Photonics (SPI) and the University of Southampton [4]. Fiber lasers provide high coherence and a narrow

beam width in a very compact configuration. Their all-fiber nature provides very high compatibility and easy integration, especially with other optical fiber systems (e.g., telecommunication systems). They have high efficiency, high gain and low thresholds. Finally, by changing the rare-earth doping element, a wide range of laser wavelengths can be achieved. For example, Thulium and Erbium both have emission spectra in the UV (10 nm – 400 nm) range as well as in the mid-IR (2.5 μm – 4 μm) range.

Fiber lasers are also very useful as they can provide both continuous-wave (CW) and pulsed operation efficiently. CW lasers refer to those whose output powers are nearly constant over time. As such, they require high heat dissipation and an ability to withstand high levels of continuous pump power, both of which are properties of fiber lasers. Pulsed lasers, on the other hand, refer to those whose output powers fluctuate periodically over time (i.e., are 'pulsed'). They are generally created through modulation and have a series of high-intensity pulses, with very low output in between pulses. The average power of such lasers are not particularly high, however by compressing the pulse duration, terawatt and petawatt peak powers can be delivered. Fiber lasers are ideal for such operation as the high beam quality allows the output to be focused to a very small spot size, providing extremely high intensity pulses.

1.3 Need for Fluoride Fiber

In most applications of fiber lasers, silica (SiO_2) glass is used as the host medium. This is especially true for communication applications, as the loss of silica fiber is lowest around 1550 nm (as shown in Fig. 1.2), which is the center of the conventional (C) transmission window. Silica fiber also has the advantage of being a very stable and robust glass that is highly available. This leads to a large reduction in cost; indeed silica fiber can be purchased in bulk for very cheap.

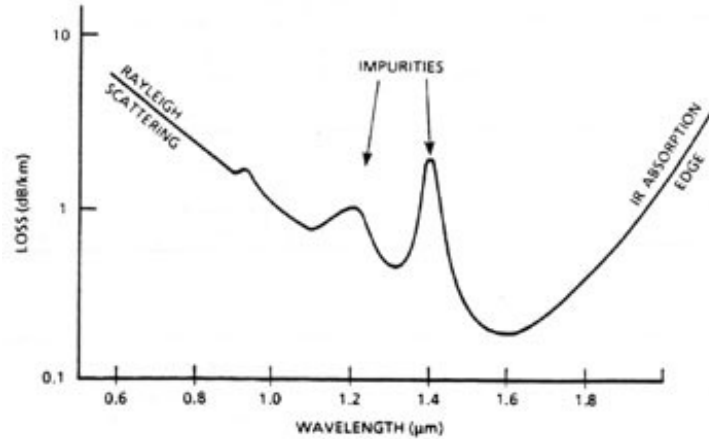


Figure 1.2: Loss profile of silica fiber [5]

Silica fiber can also be easily looped, allowing very long lengths of fiber to be assembled in a compact area. They can be very easily manipulated, and are very easy to fusion splice, allowing monolithic cavities to be created by writing the FBGs directly into the fiber. Today, passive components such as couplers, gratings and tapers are readily available in silica, and there has been considerable interest in developing more complex silica fibers for a variety of applications from sensing to supercontinuum generation.

However, depending on the application and the desired wavelength range, there can be many limitations and drawbacks to using silica as the host for fiber lasers. The work in this thesis was primarily motivated by the push towards efficient mid-IR fiber lasers. As seen in Fig. 1.2, silica fiber experiences significant loss above 1600 nm due to absorptions in the mid-IR and IR regions. This makes it unsuitable for fiber lasers when specifically targeting the mid-IR range. Its high phonon energy and low rare-earth saturation further limits its use for lasing at higher wavelengths [6]. Additionally, again due to its high phonon energy, certain excited electron energy states will have very short life-times. This will be further explained in the next chapter; however these short life-times are due to very high non-radiative decay rates and essentially prevent the use of any

transitions originating from these states (e.g., the 3H_4 state in Thulium). Due to these limitations (as well as others), the work in this thesis focuses on developing lasers in a heavy metal fluoride glass known as ZBLAN.

ZBLAN is a fluoride glass, with its name coming from the acronym formed through its chemical composition: ZrF_4 - BaF_2 - LaF_3 - AlF_3 - NaF . The elements contained are (in order): Zirconium (Zr), Barium (Ba), Lanthanum (La), Aluminum (Al) and Sodium (Na), all bonded with Fluorine. The presence of Zirconium gives ZBLAN the classification of fluorozirconate glass. It was accidentally discovered by Poulain and Lucas from the University of Rennes in 1975 [7]. Fluoride glasses, due to the presence of Fluorine, are very electronegative, giving them a strong tendency to attract electrons. They also possess much lower phonon energies than silica glass, which greatly increases the lifetime of excited dopant ions. The ZBLAN fiber used in this thesis was supplied by IRphotonics, and has an approximate loss profile as shown in Fig. 1.3. As can be seen, the low-loss range of ZBLAN fiber extends well into the mid-IR region, with suitable operation up to 4 μm . Comparing with silica, ZBLAN fiber can have losses that are 10-100 times lower throughout the mid-IR region.

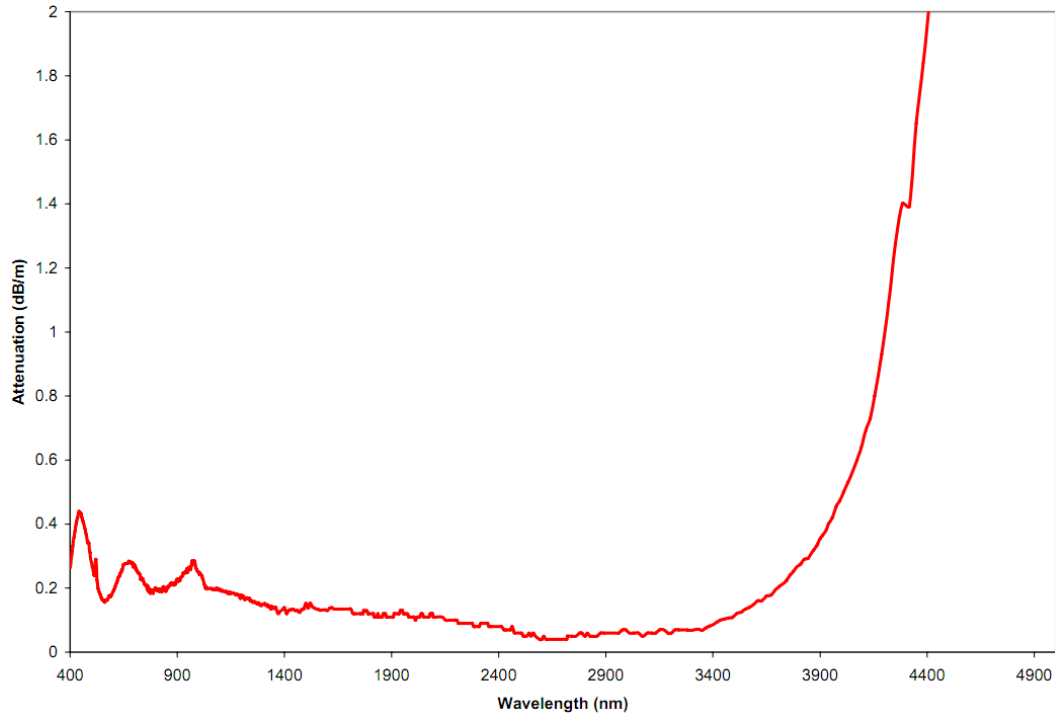


Figure 1.3: Attenuation profile of ZBLAN fiber provided by IRphotonics [8]

Other specialty glasses, for example sulphides from the chalcogenide family and tellurites from the heavy oxide family, also offer the potential for targeting the mid-IR region. Chalcogenides are mechanically stable and have a transmission window that extends far into the infrared (around 10 μm). Similar to ZBLAN, they have very low phonon energies, leading to low non-radiative decay rates. However, most applications rely heavily on their large optical non-linearity. In [9], a chalcogenide microstructured optical fiber was used to generate a fiber laser based on stimulated Brillouin scattering (SBS). Tellurites also offer an extended transmission window compared to conventional silica fiber. They have a lower phonon energy than silica, but not lower than either ZBLAN or chalcogenide fiber. More importantly, they have very high rare-earth solubility, meaning a higher concentration of ions can be doped in the fiber. However, they have low thermal conductivity and a low damage threshold, making them unsuitable for high

power fiber lasers [10]. In [11], a Thulium/Ytterbium co-doped tellurite fiber was used to create a 67 mW fiber laser with 10% slope efficiency operating at around 2 μm .

One advantage of ZBLAN fiber over both chalcogenide and tellurite fiber is that it has an index of refraction much closer to that of silica. This allows for much easier integration with SMF-28 fiber, as the loss when coupling from ZBLAN to silica will be much lower than with chalcogenide or tellurite. The main drawback with ZBLAN fiber is that it is very mechanically fragile. It is difficult to manipulate, and will break with a much smaller radius of curvature than other glasses. Additionally, it is difficult to perform splices, both ZBLAN-ZBLAN and ZBLAN-SMF.

1.4 Motivation for Mid-IR Sources

Light sources operating in the mid-IR band are extremely useful for chemical sensing and detection, as well as for many biological applications. Spectral fingerprinting can be used to qualitatively and quantitatively detect a variety of chemical species that have their peak absorption coefficients located in the mid-IR region. The absorption profiles of various chemicals (in gas phase) are shown in Fig. 1.4.

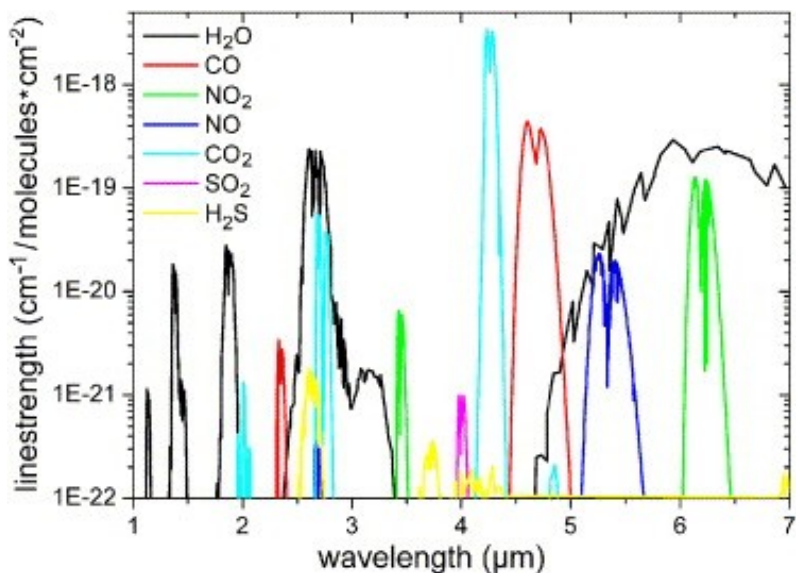


Figure 1.4: Absorption profiles of typical chemicals [12]

The simplest method for spectral fingerprinting essentially consists of passing the light beam through a desired chemical and measuring the amount of power absorbed (single-pass absorption). It is clear that placing the light source at the peak absorption of the chemical will facilitate the detection. More complex methods, such as cavity ring down spectroscopy (CRDS), can be used to facilitate the detection by passing the light through the chemical several times and measuring the decay in detected power [13]. Tissue ablation can also be facilitated through the use of mid-IR sources. Once again, due to the higher absorption, what would normally require several watts of power in the near-IR (1-2 μm) can be performed with tens of milliwatts in the mid-IR [14].

Chemical detection can be further improved through the use of dual- and multi-wavelength lasers. The idea is that most chemicals have several local absorption peaks of varying magnitude throughout the near-IR and mid-IR regions. By designing the laser wavelengths to be placed at different absorption peaks, an absorption 'pattern' can be detected. This can drastically improve the sensitivity and resolution of the detection over conventional single absorption measurements [14].

1.5 Thesis Objectives and Achievements

It is clear from the previous sections that there exists a need for mid-IR light sources (or rather a glass suitable for mid-IR applications). This need, combined with the numerous benefits, advantages, and applications of multi-wavelength fiber lasers serves as the main motivation for this thesis. The main focus of this work is on developing efficient Thulium-doped ZBLAN fiber lasers. An additional goal is on designing a multi-wavelength fiber laser and demonstrating its use for chemical detection.

This thesis will explore different fiber laser cavities and gain fiber lengths for operation at 1480 nm. This is a critical first step, as the performance of a fiber laser depends heavily on not only the configuration used, but also on the specific parameters of the gain fiber (numerical aperture, core radius, doping concentration, etc.). Therefore, the results obtained will not necessarily be the same as other reports which use gain fiber with different parameters. A Tm^{3+} :ZBLAN fiber laser emitting at 1480 nm with 32% slope efficiency and 400 mW output power is demonstrated using a 34 cm length of ZBLAN fiber, manufactured by IRphotonics with a 0.13 numerical aperture and 8,000 ppm doping concentration. The optimum lasing cavity is formed by a FBG (99.26% reflectivity) on one end and a cleaved facet (4% reflectivity due to Fresnel reflection) on the other end, with the gain fiber being pumped through a wavelength division multiplexer (WDM). The information gained from this investigation is important when moving forward with ZBLAN fiber lasers.

This thesis will also investigate the dynamics of multi-wavelength operation. A dual-band Tm^{3+} :ZBLAN fiber laser operating simultaneously at 810/1480 nm is demonstrated. This represents the first report of a dual-wavelength fiber laser which uses two lasing transitions that share the same upper energy level ($^3\text{H}_4 \rightarrow ^3\text{H}_6$ and $^3\text{H}_4 \rightarrow ^3\text{F}_4$).

We then continue the investigation by developing a three-wavelength fiber laser operating at 1460/1503/1873 nm. This laser was created in order to detect varying concentrations of water in acetone, and thus the wavelengths were chosen accordingly. There have been several reports of multi-wavelength fiber lasers, in both silica and ZBLAN, however none of the previous reports made any attempt to apply the multi-wavelength functionality for chemical detection or sensing. Single-pass absorption measurements were performed using the three-wavelength laser on 12 samples of water in acetone, with water concentrations ranging from 0.55 M to 11.4 M. A detection limit of 2.8 M was observed, and molar absorptivities were calculated to be within 10-20 % of the theoretical values.

1.6 Publications

The results presented on the dual-band Tm^{3+} :ZBLAN fiber laser (chapter 4) have been reported in the following two conferences presentations:

K. Ramaswamy, C. Jia, M. Dastmalchi, L. R. Chen, and M. Saad, "Dual-band 800/1480 nm Tm^{3+} :ZBLAN fiber laser," IEEE Photonics Conference, 8-12 September 2013, Bellevue, WA

K. Ramaswamy, C. Jia, M. Dastmalchi, B. Frison, A. R. Sarmani, L. R. Chen, and M. Saad, "Dual-wavelength Tm^{3+} :ZBLAN fiber lasers," Workshop on Specialty Optical Fibers, 28-30 August 2013, Sigtuna, Sweden

Furthermore, the results presented on the three-wavelength Tm^{3+} :ZBLAN fiber laser and the subsequent single-pass absorption measurements on water in acetone (chapter 5) have been reported in the following conference and journal publications:

C. Jia, **K. Ramaswamy**, L. Chen, A. MacLean, N. Andrews, J. Saunders, J. Barnes, H.-P. Loock, M. Saad, "Three-Wavelength Tm³⁺:ZBLAN Fiber Laser and its Applications in Water Detection," IEEE Photonics Conference, 12-16 October 2014, San Diego, CA

N. Andrews, A. MacLean, J. Saunders, J. Barnes, H.-P. Loock, C. Jia, **K. Ramaswamy**, L. R. Chen, "Quantification of Different Water Species in Acetone Using a NIR-Triple-Wavelength Fiber Laser," Optics Express, vol 22, Issue 16, pp. 19337-19347 (2014)

1.7 Outline of Thesis

The remainder of the thesis is organized as follows. In chapter 2, an overview of the lasing transitions in Thulium ions is presented, along with some potential applications of Thulium-doped fiber lasers. Following this, a review of single- and multi-wavelength Thulium-doped ZBLAN fiber lasers is presented.

Chapters 3 and 4 explore single-wavelength lasing at 1480 nm and dual-band lasing at 810/1480 nm, respectively. Both chapters include a background on the applications of such a laser, the experimental setup used for the measurements and the experimental results obtained.

Chapter 5 describes the design of a triple wavelength laser operating at 1460/1503/1873 nm and its use for detecting water in acetone. Laser characterization is performed, and the results from single-pass absorption measurements on various samples of water in acetone are presented.

The thesis concludes with a summary of the results presented and a discussion of future investigations.

Chapter 2 Background

This section presents a background on single and multi-wavelength Thulium-doped ZBLAN fiber lasers. In section 2.1, the use of Thulium as a rare-earth dopant is explained, along with an overview of other possible rare-earth elements. Following this in section 2.2, a review of dual- and multi-wavelength Thulium-doped fiber lasers is presented. Finally, in section 2.3, a summary of the chapter is given.

2.1 Rare-Earth Elements

2.1.1 Introduction

Fiber lasers use doped optical fibers as the gain medium. While there is a choice for the type of glass (silica, ZBLAN, chalcogenide etc.), there is also a choice for the doping element. Typically, rare-earth elements – defined as elements 57 (Lanthanum) to 71 (Lutetium) on the periodic table – are used. These elements are classified as the ‘lanthanides’, and have an electron configuration which makes them more appealing for fiber laser applications than transition metals or other elements [6]. Although the first fiber laser was doped with Neodymium, the most common rare-earth elements used today are Erbium, Ytterbium, and Thulium.

The electronic configuration for lanthanide elements are of the form $[\text{Xe}]4f^n6s^2$, where n varies depending on the element. They all share the property of having a $6s^2$ valence layer and an incomplete $4f$ shell. The optical transitions will therefore take place in this $4f$ shell, which is closer to the core and thus partially shielded from the local environment.

When doped in a glass matrix, lanthanide elements lose three electrons: the two outer electrons from the 6s shell and one electron from the 4f shell [15]. For example, the configuration of Thulium goes from $[\text{Xe}]4f^{13}6s^2$ to $[\text{Xe}]4f^{12}$ when it is doped in glass. The 5s, 5d and 5f shells remain intact and thus the shielding on the 4f shell is still present. Lanthanide elements doped in a glass therefore behave similarly to their trivalent ion form (in this case Tm^{3+}). It is therefore common to use the trivalent ion name when defining a doped fiber; for example a Thulium-doped ZBLAN fiber is named Tm^{3+} :ZBLAN.

2.1.2 Thulium

As previously mentioned, many different rare-earth elements can be used to create fiber lasers. However, this thesis focuses specifically on Thulium (doped in ZBLAN glass). The characteristics of a fiber laser doped with Thulium are based on the properties of the element in its trivalent form, i.e., based on the spectroscopic properties of Tm^{3+} ions. To examine these properties we must look at the valence layer of these ions, i.e., the $4f^{12}$ layer. From Laporte's selection rule, electronic transitions are normally only allowed for energy states with opposite parities [6]. The energy states of free Tm^{3+} ions have the same parity, as they are in the same orbital, and thus electronic transitions are not permitted. However, when Tm^{3+} ions are doped into a glass (silica, ZBLAN etc.), the coupling between the 4f and 5d subshells causes a mixing of opposite parity energy states, which allows certain electronic transitions to be allowed within the 4f shell [15]. The electronic transition diagram for Tm^{3+} ions in a glass host is shown in Fig. 2.1.

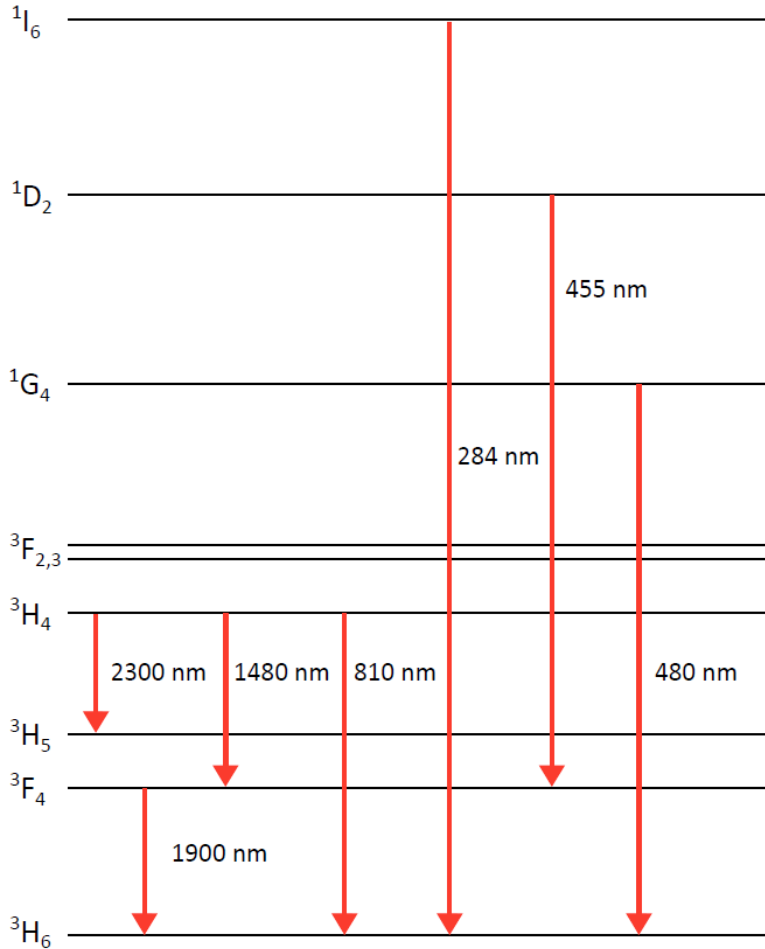


Figure 2.1: Electronic transitions of Tm³⁺ ions [6]

The transitions shown in Fig. 2.1 represent radiative transitions, i.e., transitions which release photons. However, there are also non-radiative transitions in which electrons decay to a lower energy state without releasing any photons (the energy is released as vibrational motion). Details on this will be presented in the following section.

In order for an electronic transition to generate lasing, a population inversion between the two transition states must be created. A population inversion refers to a higher population of electrons in the upper level of the transition than in the lower level of the transition. For this to occur, the rate at which the upper level is populated must be much faster than the emission rate of the transition. A three-level laser is shown in Fig.

2.2. The fast transition from level 3 to level 2 along with the slow transition from level 2 to level 1 causes a buildup of electrons in the upper transition level (level 2) creating a population inversion.

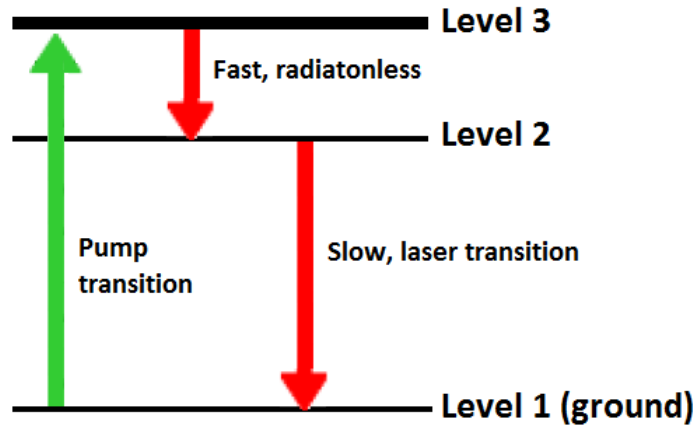


Figure 2.2: Three-level laser example showing fast and slow transitions

The rates of the different transitions depend heavily on the host glass, and more specifically on the phonon energy of the host glass. Glasses with a high phonon energy lead to certain energy states having a very short life time (due to fast non-radiative decay rates) making lasing difficult to obtain, while glasses with a low phonon energy allow lasing for a much larger number of transitions.

In a silica host, Tm^{3+} ions are mainly used for lasing around 1900 nm through the ${}^3F_4 \rightarrow {}^3H_6$ transition. A laser operating at 1900 nm can serve as a pump source for a holmium-doped fiber laser; indeed, a tunable Holmium-doped fiber laser operating around 2120 nm with greater than 15 W output power has been demonstrated using a Thulium-doped fiber laser at 1950 nm [16]. In this case, the 3F_4 level was populated by first exciting the 3H_4 state through pumping at 790 nm. In a silica host, the 3H_4 state has a very short life-time (14.2 us) and will rapidly decay non-radiatively to the 3H_5 state. In Tm^{3+} ions, the 3H_5 state also has a very fast non-radiative decay rate and thus electrons will drop to 3F_4 very quickly. Population inversion is maintained as the ${}^3H_4 \rightarrow {}^3H_5$ and 3H_5

→ 3F_4 non-radiative transitions are much faster than the ${}^3F_4 \rightarrow {}^3H_6$ radiative transition. Direct excitation of the 3F_4 level can also be obtained through pumping at 1575 nm, albeit with a lower efficiency.

In a fluoride host, many more lasing transitions are available for Tm^{3+} ions. Many of these transitions originate from the 3H_4 level, and lasing is made possible because this energy state has a life-time of 1350 μs in ZBLAN – almost two magnitudes larger than in silica [17]. The ${}^3H_4 \rightarrow {}^3H_5$ transition is used for lasing around 2300 nm, the ${}^3H_4 \rightarrow {}^3F_4$ transition is used for lasing around 1480 nm and the ${}^3H_4 \rightarrow {}^3H_6$ transition is used for lasing around 810 nm. Lasing around 1900 nm is also possible in ZBLAN; in fact a comparison was done in 2004 by Walsh and Barnes and it was reported that using ZBLAN glass instead of silica would provide slope efficiencies that were two times as high [17]. A further study by Eichhorn and Jackson in 2008 showed that while the fluoride fiber still had higher slope efficiency, the performance was comparable with silica [18]. Fig. 2.3 shows the output power vs. pump power for optimized lengths of ZBLAN and silica fiber.

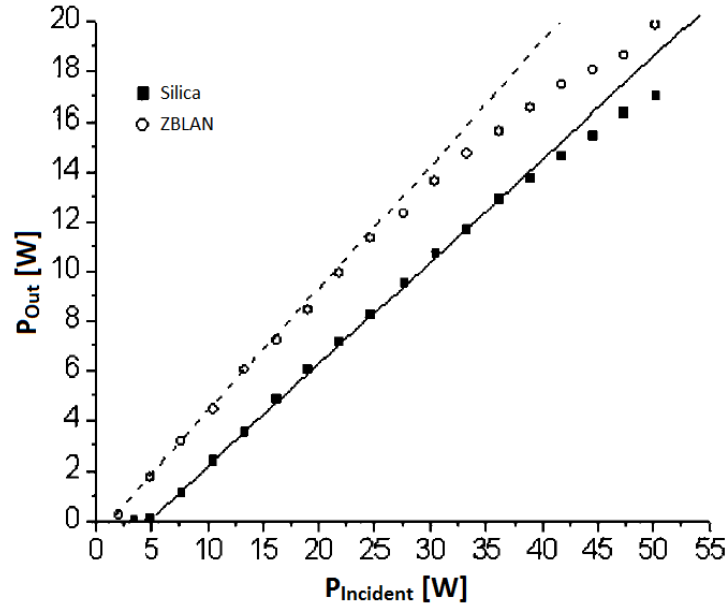


Figure 2.3: Comparison of output power vs. incident power for a Tm³⁺:silica fiber laser (square) and a Tm³⁺:ZBLAN fiber laser (circle) operating at 1900 nm [18]

Lasing around 2300 nm is in the mid-IR range and has many applications as presented in the previous chapter, while lasing around 1480 nm is of particular interest as it can serve as a pump for Er³⁺ ions. However, both of these transitions suffer from a bottleneck problem at the ³F₄ level (the ³H₅ level rapidly decays to the ³F₄ level) when the ³H₄ level is directly pumped at 790nm. The rate at which electrons return to the ground state from the ³F₄ level is almost 5 times slower than the ³H₄ → ³F₄ laser transition [19]. This causes a buildup of electrons in the ³F₄ level, making population inversion impossible to maintain. This is known as a self-terminating transition as lasing can only be established for a short time before it must be turned off in order to allow the ³F₄ level to de-populate.

There are two main solutions to this problem; the first is by co-lasing at 1900 nm [20]. This allows the ³F₄ level to be de-populated through the ³F₄ → ³H₆ transition, enabling a population inversion for the ³H₄ → ³F₄ and ³H₄ → ³H₅ → ³F₄ transitions. The

second (and more common) solution is to use a 3-level up-conversion pumping configuration, as shown in Fig. 2.4.

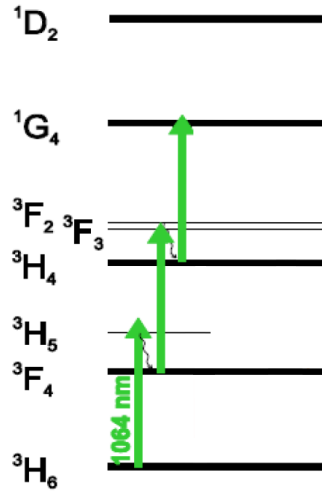


Figure 2.4: Up-conversion pumping at 1064 nm in Tm³⁺ ions

In this case, a 1064 nm pump is used, and the ³H₄ level is populated through a two-step process: ground state electrons are first excited to the ³F₄ level (³H₆ → ³H₅ with a fast, non-radiative, ³H₅ → ³F₄) followed by a second excitation and fast non-radiative decay (³F₄ → ³F_{2/3} and ³F_{2/3} → ³H₄). This allows the ³F₄ state to be sufficiently depopulated in order to produce a population inversion for the radiative ³H₄ → ³F₄ transition. Using this pump configuration, a 150 mW Tm³⁺:ZBLAN fiber laser emitting at 2300 nm was reported [21]. A 2 m length of 1,000 ppm ZBLAN fiber was used, and 8% slope efficiency was obtained, as shown in Fig. 2.5. The same pump configuration was also used to demonstrate a high-power, high-efficiency Tm³⁺:ZBLAN fiber emitting at 1480 nm [22]. A maximum output power of 2.3 W with 65% slope efficiency was obtained. The output power vs. pump power curve is shown in Fig. 2.6, with the dotted line representing experimental results and the solid line representing simulated results.

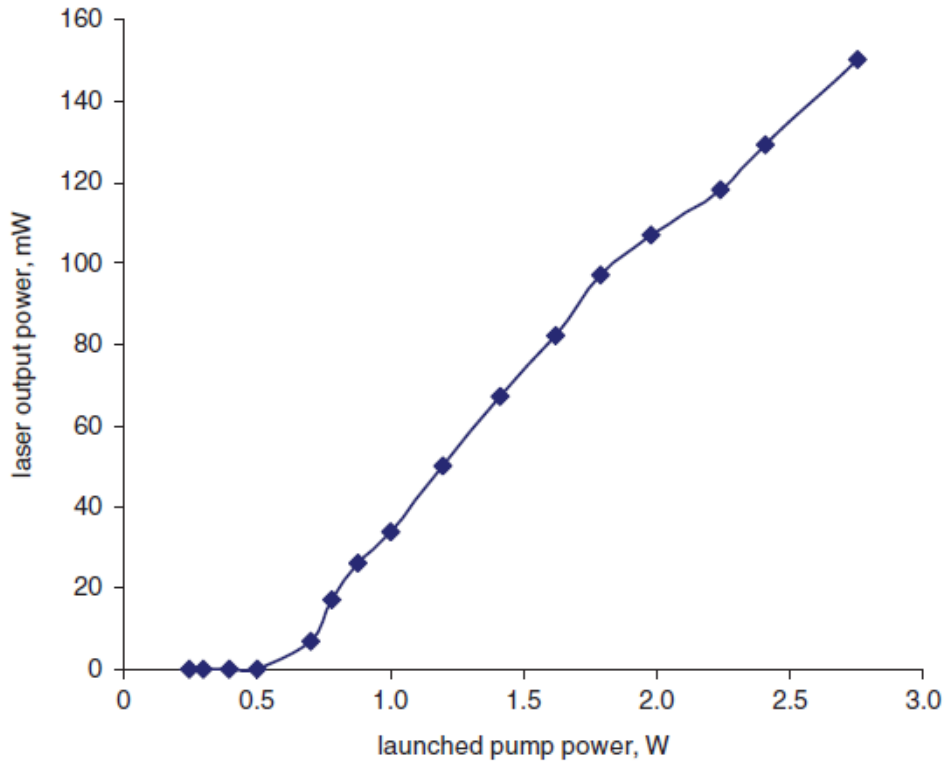


Figure 2.5: Output power vs. pump power for a 2300 nm Tm³⁺:ZBLAN fiber laser [21]

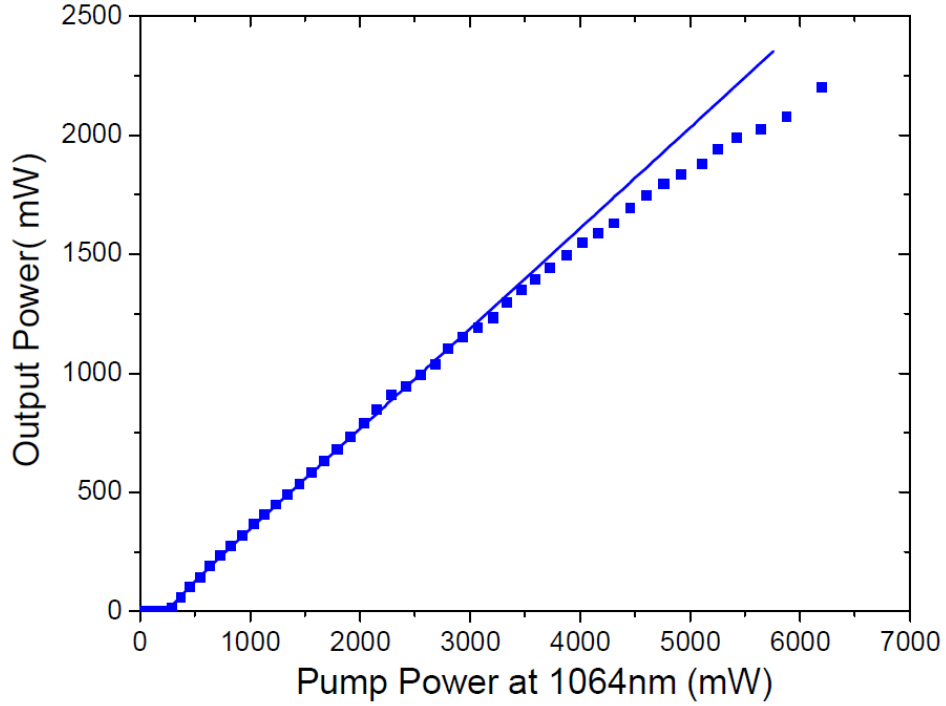


Figure 2.6: Experimental (dotted) and simulated (solid) output power vs. pump power curves for a 1480 nm Tm³⁺:ZBLAN fiber laser [22]

Lasing around 810 nm is noteworthy as this is in the first telecommunication window. It can be achieved using either of the two pump methods previously described; the $^3H_4 \rightarrow ^3H_6$ transition returns electrons directly to the ground state thus avoiding any bottleneck issue at the 3F_4 level. It was first demonstrated in ZBLAN fiber by Allain *et al.* in 1989 [23]. The gain fiber was pumped at 676.4 nm, and lasing was achieved at a threshold of 45 mW, with 1.6% slope efficiency and a maximum output power of 0.5 mW. A high power Tm^{3+} :ZBLAN fiber laser was demonstrated by Dennis *et al.* through up-conversion pumping at 1064 nm [24]. They obtained 1.2 W continuous-wave (CW) output power with 33% slope efficiency, as shown in Fig. 2.7.

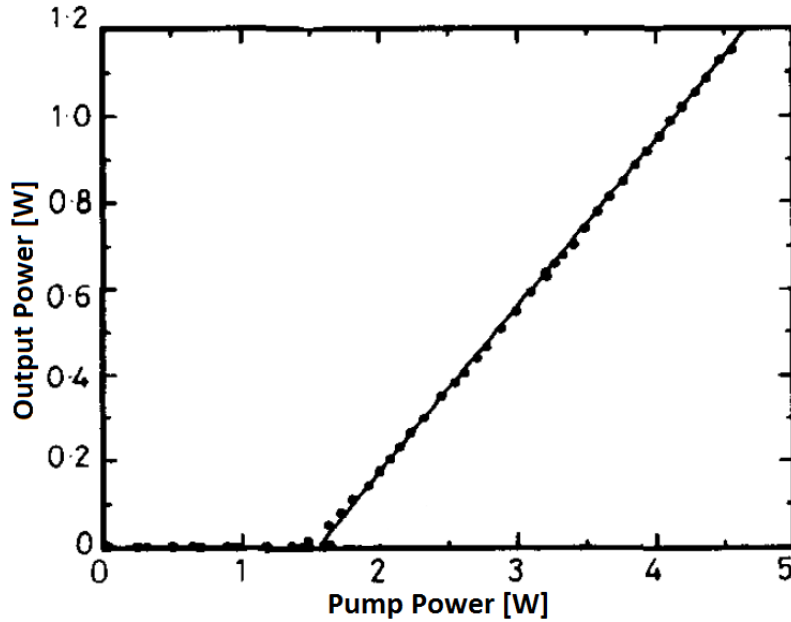


Figure 2.7: Output power vs. pump power for a 810 nm Tm^{3+} :ZBLAN fiber laser [24]

Several blue and ultraviolet transitions are also available with Tm^{3+} ions ($^1I_6 \rightarrow ^3H_6$, $^1D_2 \rightarrow ^3F_4$, $^1G_4 \rightarrow ^3H_6$). However, some care must be taking when utilizing these transitions as they can lead to photodarkening in the fiber [15]. This effect can occur during high energy transitions and can lead to a saturation of the laser output power and a reduction in the lifetime of the fiber.

The focus of this thesis is on Thulium-doped fiber lasers. However, many other rare-earth elements can be used to create fiber lasers. The electronic transition diagrams for Er^{3+} , Yb^{3+} and Nd^{3+} ions are included in Appendix A, along with brief highlights for each one.

2.3 Review of multi-wavelength Tm^{3+} :ZBLAN Fiber Lasers

This section presents a review of relevant multi-wavelength Tm^{3+} :ZBLAN fiber lasers. This area has been well researched as the applications of such lasers are numerous, ranging from spectroscopy to telecommunications to biology and medicine. Techniques such as cavity ring-down spectroscopy can be employed with the use of multi-wavelength fiber laser. Additionally, even single-pass spectroscopic measurements can be enhanced by measuring the absorption simultaneously at multiple wavelengths, as any wavelength shift of the target chemical due to the host can be addressed. Further details on the applications of dual and multi-wavelength fiber lasers are included in chapters 4 and 5.

There have been several reports of multi-wavelength Tm^{3+} :ZBLAN fiber lasers emitting around 785 and 810 nm [27-29]. These fibers were up-conversion pumped around 1110 nm to excite electrons up to the $^3\text{H}_4$ and $^1\text{G}_4$ states, and achieved lasing around 785 nm and 810 nm through the $^3\text{H}_4 \rightarrow ^3\text{H}_6$ and $^1\text{G}_4 \rightarrow ^3\text{H}_5$ transitions, respectively, as shown in Fig. 2.8. In [28], single, dual- and three-wavelength lasing were all observed by varying the spacing between the fiber and the mirror on one end. As shown in Fig. 2.9, by increasing the spacing the operation shifts from dual-wavelength to three-wavelength before eventually going to single-wavelength.

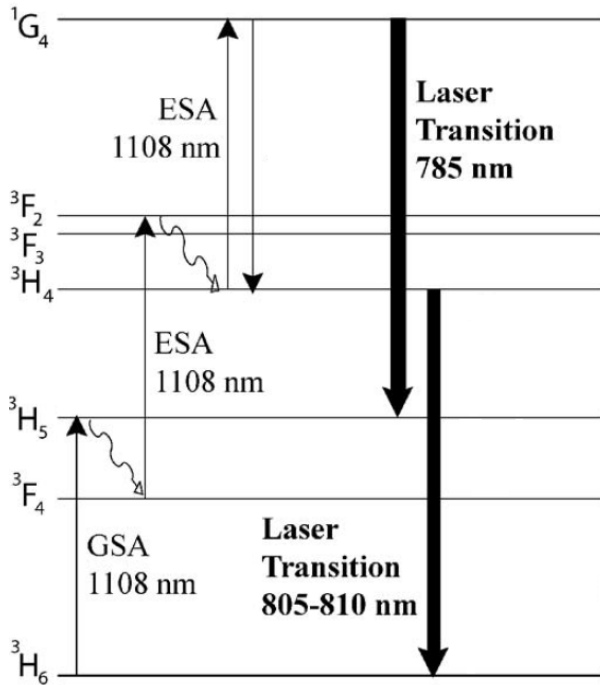


Figure 2.8: Transition diagram for dual-wavelength emission at 785 nm and 810 nm [27]

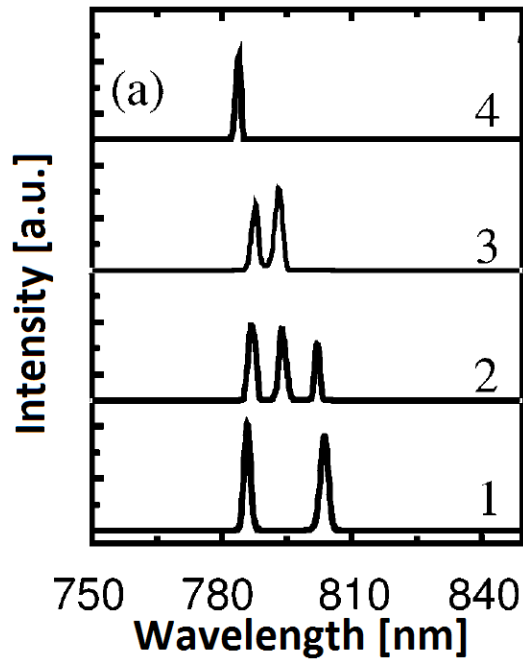


Figure 2.9: Multi-wavelength spectrum around 785 and 810 nm [28]

In [27], a self-pulsing phenomenon was observed and was attributed to gain competition between two laser transitions. The self-pulsing dynamics were seen as soon as both transitions were lasing simultaneously.

Dual-wavelength lasing around 800 nm using a single transition, namely the ${}^3\text{H}_4 \rightarrow {}^3\text{H}_6$ transition, has been demonstrated [30]. Up-conversion pumping at 1064 nm was used to excite the ${}^3\text{H}_4$ state, while the cavities were created by two highly reflective FBGs and a shared Fresnel reflection air gap. The reflection is created at the silica-air interface and is due to a difference in indices of refraction of the two mediums. Simultaneous dual-wavelength operation at around 5 mW was achieved for pump powers around 900 mW, as shown in Fig 2.10. The same group also demonstrated dual-wavelength lasing around 1480 nm using the ${}^3\text{H}_4 \rightarrow {}^3\text{F}_4$ transition [31]. A similar cavity and pumping configuration was used and both single and dual-wavelength operations were achieved. Wavelength switching was demonstrated and a wavelength spacing as narrow as 0.6 nm was observed, as shown in Fig 2.11.

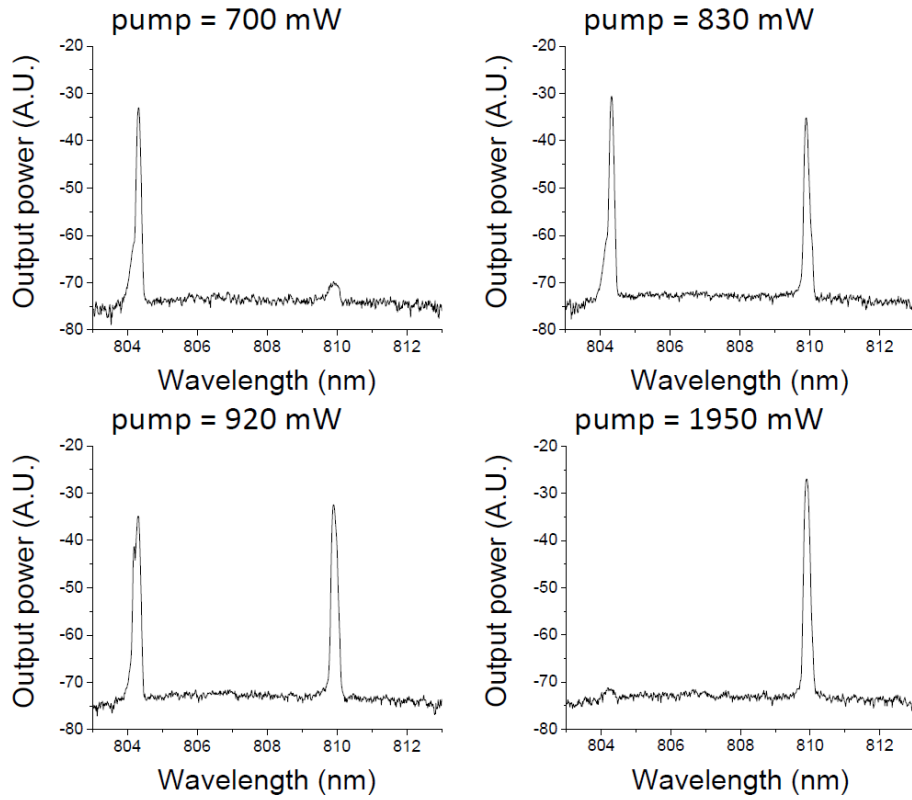


Figure 2.10: Dual-wavelength Tm^{3+} :ZBLAN fiber laser operating around 800 nm [30]

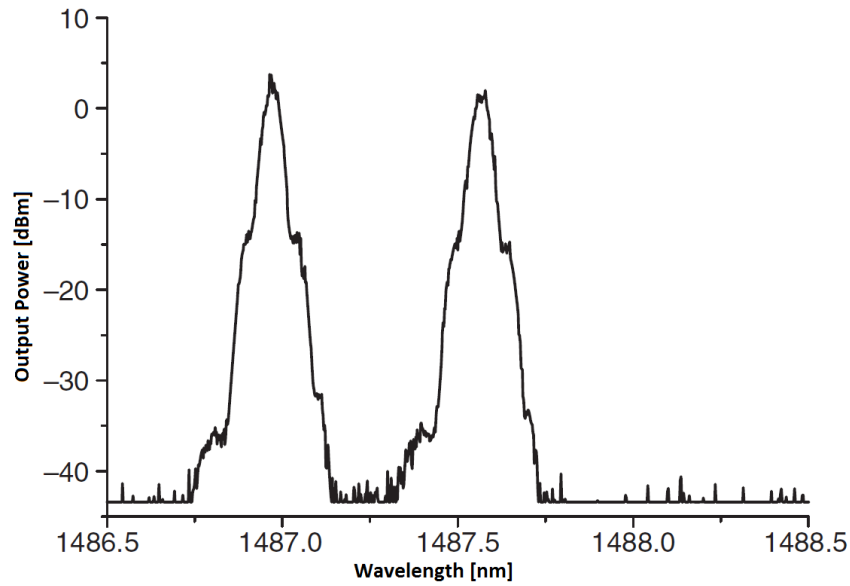


Figure 2.11: Dual-wavelength Tm^{3+} :ZBLAN fiber laser operating around 1480 nm [31]

2.3 Summary

The purpose of this chapter was to introduce rare-earth doped fibers and show how they can be used to make efficient fiber lasers. To this extent, sections 2.1 explored the transitions of Tm^{3+} ions and provided examples on lasing in both silica and ZBLAN fiber. This included single-wavelength lasing around 810 nm, 1480 nm, 1900 nm, 2300 nm, as well as certain UV wavelengths. Following this, section 2.2 presented a review of relevant multi-wavelength Tm^{3+} :ZBLAN fiber lasers. This included dual-wavelength at 785 and 810 nm, dual-wavelength around 810 nm and dual-wavelength around 1480 nm. The remaining chapters in this thesis present the experimental results from single-wavelength lasing at 1480 nm, dual-band lasing at 810/1480 nm and a triple-wavelength fiber laser emitting simultaneously at 1460/1503/1873 nm.

Chapter 3 Lasing at 1480 nm

This chapter presents the experimental results obtained from lasing at 1480 nm in a Tm^{3+} :ZBLAN fiber laser. The chapter begins with a motivation for 1480 nm fiber lasers, as well as a review of possible up-conversion pump configurations. Section 3.2 then covers details concerning the experimental setup used to obtain the results. Section 3.3 provides an analysis of the results obtained in this chapter. Finally, section 3.4 concludes the chapter with a summary of the results and a brief discussion on ways to improve the performance.

3.1 Introduction

High power fiber lasers operating at 1480 nm can be very appealing to use as pump sources for Erbium-doped fiber amplifiers (EDFA) and Raman fiber amplifiers (RFA), both of which play a vital role in modern day fiber optic networks. They offer lower noise levels than pump sources operating at 980 nm, and have higher efficiencies than typical laser diodes [22]. Lasing at 1480 nm in Tm^{3+} :ZBLAN fiber can be obtained through the transition between two excited states, namely ${}^3\text{H}_4 \rightarrow {}^3\text{F}_4$. Direct pumping of electrons to the ${}^3\text{H}_4$ state is possible, either by pumping at 674 nm or by pumping at 790 nm. In [23], a krypton-ion laser at 676.4 nm was used as the pump source to obtain CW lasing at 1480 nm. However, since the transition is self-terminating, population inversion is difficult to achieve and the conversion efficiency was very low (tens of μW from $40 \text{ mW} \leq 1\%$).

One of the main solutions to the self-terminating ${}^3\text{H}_4 \rightarrow {}^3\text{F}_4$ transition is to depopulate the ${}^3\text{F}_4$ level by co-lasing at 1900 nm through the ${}^3\text{F}_4 \rightarrow {}^3\text{H}_6$ transition. Indeed, in [32], co-lasing at 1480 nm and 1900 nm is achieved by using a Ti:sapphire laser at 790

nm as the pump source and two mirrors coated for reflectivity at 1460 nm and 1860 nm. Conversion efficiencies of 16% and 25% at 1460 nm and 1860 nm, respectively, were achieved using 145 mW of pump power. However, as was described in chapter 2, a more common solution is to use up-conversion pumping to de-populate the 3F_4 level, as shown in Fig. 3.1.

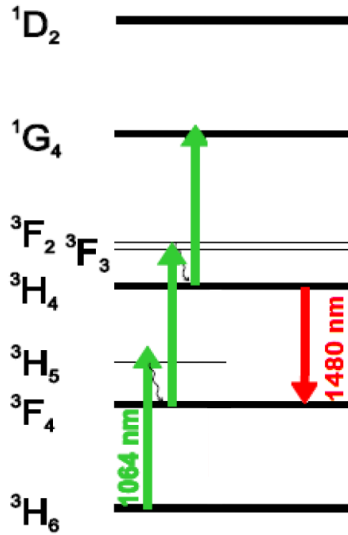


Figure 3.1: Upconversion pumping at 1064 nm to produce 1480 nm lasing

This configuration was first proposed by Komukai *et al.* in 1995 and has become a common single-wavelength up-conversion pumping approach [33]. However, there have been many reports of using additional pumps to improve the up-conversion pumping efficiency.

In [34], an additional pump at 1560 nm was used, as shown in Fig. 3.2a. This was done for two reasons: to increase the population of the 3F_4 state (which would then be further excited to the 3H_4 state) and to remove additional ground-state electrons. The absorption cross-section at 1560 nm is much larger than at 1064 nm, and thus the first stage of the up-conversion process can be greatly enhanced by adding radiation at 1560 nm with about 10% of the 1064 nm pump power, making the population inversion more

efficient. An added effect of increasing the population of the lower laser level is that the peak gain is shifted from 1460 nm to around 1500 nm. Finally, by removing additional ground-state electrons, the absorption around 1500 nm can be reduced. In [35], a second pump source at 1410 nm was added in order to facilitate the second stage of the up-conversion process, as shown in Fig. 3.2b. The added pump serves to further depopulate the 3F_4 level and excite additional electrons to the upper 3H_4 laser level. A slope-efficiency of 12.5 % was obtained using a Thulium-doped silica fiber, which is quite impressive considering the short life-time of the 3H_4 state in silica. Using a fluoride glass host with this pumping configuration would produce even better results. Not surprisingly, a third dual-wavelength up-conversion pumping configuration involves using pump sources around 1064 nm and 800 nm, as shown in Fig. 3.2c. In [36], a Ytterbium-doped fiber laser at 1050 nm and a Ti:Sapphire laser at 800 nm was used in a Thulium-doped ZBLAN fiber amplifier. The 800 nm pump was used to directly excite the upper 3H_4 level with a high GSA cross-section, while the 1064 nm pump was used to de-populate the lower 3F_4 level due to a strong ESA cross-section (and also further populate the 3H_4 level). A gain enhancement of about 20 dB was demonstrated through the addition of the 800 nm pump.

An additional pumping scheme which deserves attention is a combination of 1560 nm and 1410 nm, as shown in Fig. 3.2d. The pump at 1560 nm uses the $^3H_6 \rightarrow ^3F_4$ transition to populate the lower laser level, while the pump at 1410 nm uses the $^3F_4 \rightarrow ^3H_4$ transition to populate the upper laser level while also de-populating the lower level. One immediate advantage of this configuration is that it avoids the unwanted $^3H_4 \rightarrow ^1G_4$ excitation. Promoting electrons to the 1G_4 state can lead to photodarkening through the high-energy $^1G_4 \rightarrow ^1H_6$ radiative decay [25]. Therefore, a pump configuration which avoids exciting the 1G_4 state would likely improve the lifetime of the fiber laser. This

pumping scheme has been used in [37] to create a gain-shifted Thulium-doped fiber amplifier, and has been shown in [38] to have a better performance than using a 1064/1560 nm combination for amplification around 1500 nm.

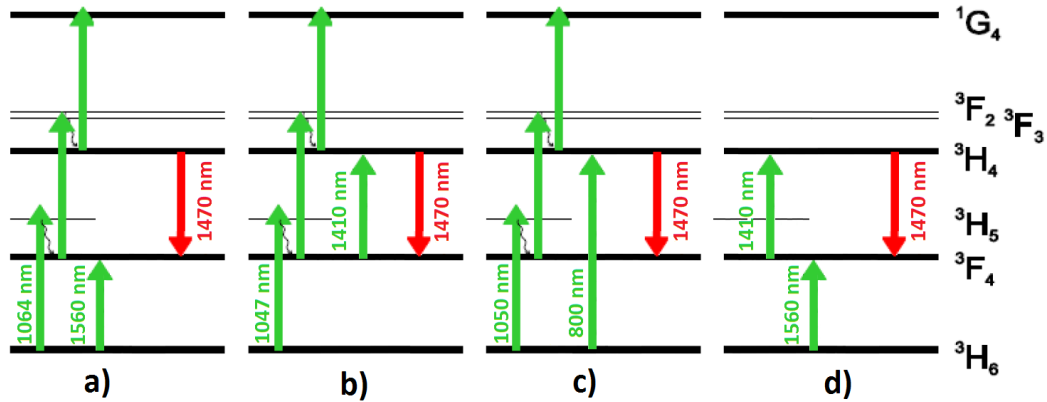


Figure 3.2: Dual-wavelength up-conversion pump configurations at a) 1064/1560 nm b) 1047/1410 nm c) 1050/800 nm d) 1410/1560 nm

This chapter is based on single-wavelength up-conversion pumping at 1064 nm. This was chosen mainly for simplicity and to reduce the number of pump sources required. The goal is to gain a better understanding of the ZBLAN gain fiber that will be used throughout the thesis. As previously mentioned, the performance of a fiber laser depends heavily on the parameters of the gain fiber (i.e., doping concentration, core radius, etc.). This chapter attempts to characterize the gain fiber and determine optimum laser configurations and gain fiber lengths.

3.2 Experimental Setup

The schematics for the different laser cavities investigated are shown in Fig. 3.3 and in Fig. 3.4. In all cases, the gain medium is a single length of double-cladding Tm^{3+} :ZBLAN fiber manufactured by IRphotonics. The doping concentration of Tm^{3+} ions is 8,000 ppm, the core diameter is 8 μm , and the cladding diameter is 125 μm with a 15 μm fluoroacrylate and acrylate coating. The pump source is a Ytterbium-doped fiber laser

(YDFL) which provides up-conversion pumping at 1064 nm. The YDFL is controlled by an external Agilent E3634 DC power supply.

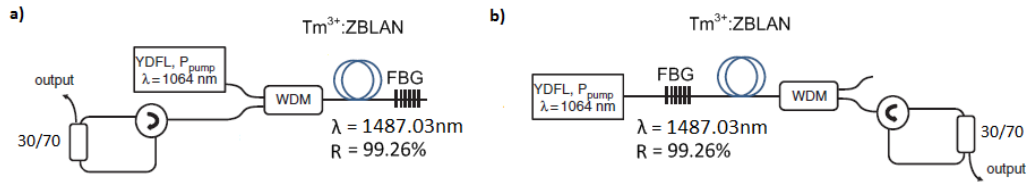


Figure 3.3: Laser cavity with a loop mirror a) Pumping through the WDM coupler b) Pumping through the FBG

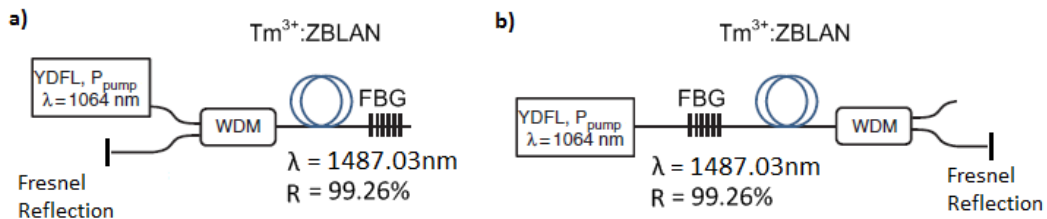


Figure 3.4: Low-loss laser cavity a) Pumping through the WDM coupler b) Pumping through the FBG

In Fig. 3.3, the cavity is formed on one end by a fiber Bragg grating (FBG) written in SMF-28 fiber and on the other end by a loop mirror created through a combination of a circulator with a 30/70 coupler. The center wavelength of the FBG is $\lambda = 1487.03$ nm with a bandwidth $\Delta\lambda = 0.4$ nm and the reflectivity is 99.26%. The FBG has an insertion loss of 1 dB, while the total cavity insertion loss of the circulator and coupler combination is approximately 2.5 dB. One branch of the 30/70 coupler is used to extract the output, while the other branch completes the loop mirror. Two measurements are thus taken; one with the 30% branch extracting the output and one with the 70% branch extracting the output. A 1064/1480 wavelength division multiplexer (WDM) coupler is used to separate the pump signal at 1064 nm from the lasing signal at 1487 nm. In Fig. 3.3a, the gain fiber is pumped through the 1064 nm port on the WDM coupler, while in Fig. 3.3b, the gain fiber is pumped directly through the FBG.

In Fig. 3.4, the loop mirror is replaced with a 4% Fresnel air reflection from a cleaved facet (in SMF-28 fiber). In this case, the cleaved facet serves as a 96% output coupler. This configuration has a lower cavity insertion loss as the loop mirror has been removed. The Fresnel reflection is created at the glass-air interface of the cleaved facet, and is caused by the different in refractive indices of the two mediums (air = 1, SiO₂ = 1.458). The remainder of the cavity is the same, with Fig. 3.4a once again pumping through the WDM coupler and Fig. 3.4b pumping directly though the FBG. Only one measurement is taken in this case, as the 30/70 coupler has been removed.

In all configurations, two mechanical splices (one on each end) are used to connect the ZBLAN fiber to the silica fiber. At the time that these measurements were taken, there was no reliable method for performing low-loss fusion splices of ZBLAN fiber to silica fiber. The total insertion loss of the two mechanical splices varies between 1.5-2.5 dB. Note that it is difficult to measure the exact insertion loss due to absorption in the gain fiber.

For each configuration, several different lengths of Tm³⁺:ZBLAN fiber were measured in order to determine not only the optimum configuration, but also the optimum length of gain fiber. For each measurement (i.e., one configuration and one length), the results were obtained by sweeping the external current source in steps of 0.1 A (which provided increments of 20-30 mW of pump power) and recording the corresponding output power.

3.3 Experimental Results

Each of the six configurations was measured using six different lengths of ZBLAN fiber: 34 cm, 40 cm, 52 cm, 60 cm, 85 cm, and 140 cm. From each output power vs. pump power measurement, two parameters are extracted: the threshold pump power

and the conversion efficiency. The threshold pump power is defined as the minimum pump power for which lasing occurs (i.e., the pump power at which lasing begins). The conversion efficiency is a measure of how much pump power is being converted into signal power (in this case, at 1487 nm). It can be seen as the slope of the output power vs. pump power curve, beginning after threshold has been reached.

The pump power is taken as the power going into the ZBLAN fiber, i.e., after the WDM coupler or after the FBG. In both cases, the pump power is measured by disconnecting the gain fiber and replacing it with the power meter. This is done prior to the measurement of any output powers.

All power measurements are done using a Thorlabs thermal power meter, which can tolerate powers up to 10 W. The entire measurement is automated, with a GPIB connection controlling the current source (and thus the pump power) and a synchronized USB connection controlling the power meter.

In order to determine the optimum configuration, one length of gain fiber was taken and all six configurations were measured. The output power vs. pump power measurements using a 34 cm piece of ZBLAN fiber are shown in Fig. 3.5. The curves that are labeled 'through WDM' refer to pumping the gain fiber through the WDM coupler, while the curves labeled 'through FBG' refer to pumping directly through the FBG. The curves with '4% reflection' are the two low-loss configurations using the 4% Fresnel air reflection. Finally, the '30% to loop' curves imply that the 30% branch of the 30/70 coupler is sent to the cavity while the 70% branch is taken as the output. Similarly, the '70% to loop' curves imply that the 70% branch is sent to the cavity and the 30% branch is taken as the output.

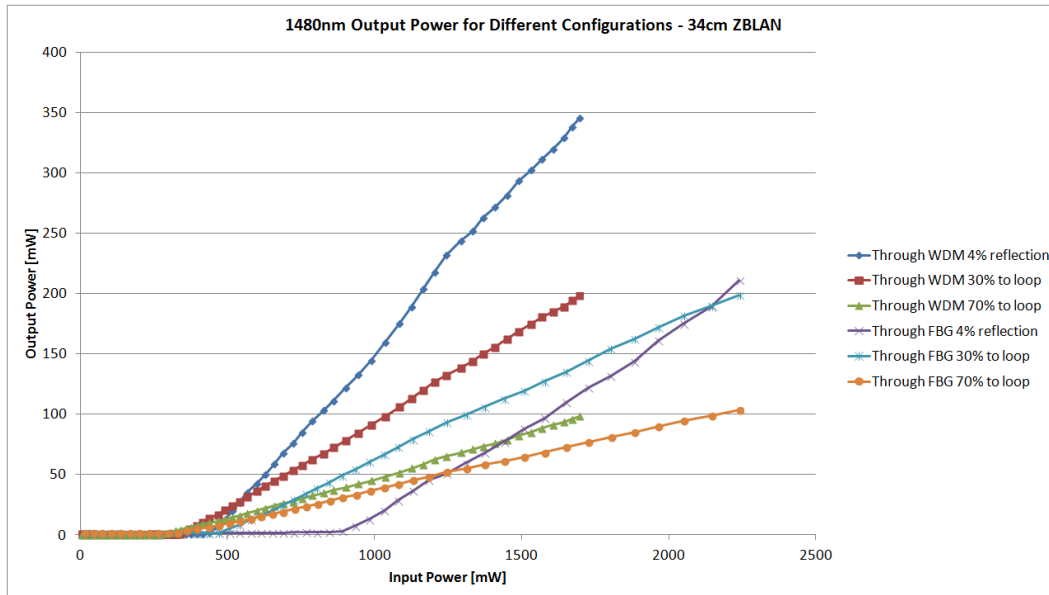


Figure 3.5: Output power for each configuration using a 34cm piece of ZBLAN fiber

We can see in Fig. 3.5 that although the threshold is slightly higher, the maximum efficiency and maximum output power are obtained from the configuration in which the gain fiber is pumped through the WDM coupler and uses a 4% Fresnel air reflection for the cavity. Furthermore, we can see that when using the loop mirror in the cavity, sending the higher percentage (70%) back into the cavity provides a lower threshold power, while sending the lower percentage (30%) into the cavity provides higher conversion efficiency. In fact, all of the lengths show a similar trend of high conversion efficiency when using the Fresnel reflection and low threshold power when using the loop mirror with the 70% branch directed to the cavity. These results are summarized at the end of this section.

In order to determine the optimum length, we use the high conversion efficiency configuration (pumping through WDM coupler with 4% Fresnel reflection) and measure the six different lengths of gain fiber. The output power vs. pump power measurements

are shown in Fig. 3.6, and the threshold powers and conversion efficiencies are shown in Table 3.1.

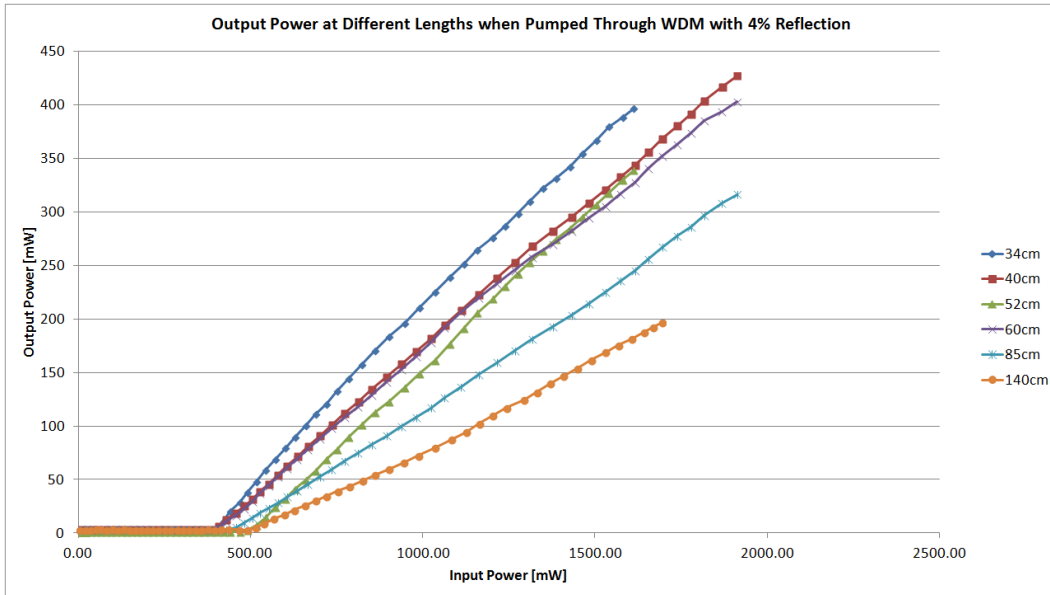


Figure 3.6: Output power vs. Input power curves for different lengths using high conversion efficiency configuration

Table 3.1: Threshold and slope efficiency for different lengths using optimum high conversion efficiency configuration

Length [cm]	Threshold [mW]	Slope Efficiency (%)
34	401.70	32.2
40	406.62	28.1
52	491.07	30.6
60	406.62	26.7
85	456.56	21.4
140	516.09	16.4

We can see from the results shown in Table 1 that the highest conversion efficiency and lowest threshold power come from using the 34 cm length of ZBLAN gain fiber. However, it is important to note that each length of fiber uses its own pair of mechanical splices with varying insertion losses. It is therefore difficult to make an exact comparison of the different lengths, as each case will have a slightly different cavity loss.

Nevertheless, we can still observe a general trend of increase in threshold power and decrease in conversion efficiency as the length of the gain fiber increases.

Finally, we take a look at the spectrum of the laser at different pump power levels. A plot of the power spectral density (PSD) measured on an HP70952 optical spectrum analyzer (OSA) is shown in Fig. 3.7. This was measured from 900 nm to 1550 nm, with 0.1 nm resolution bandwidth and a sensitivity of -60 dBm.

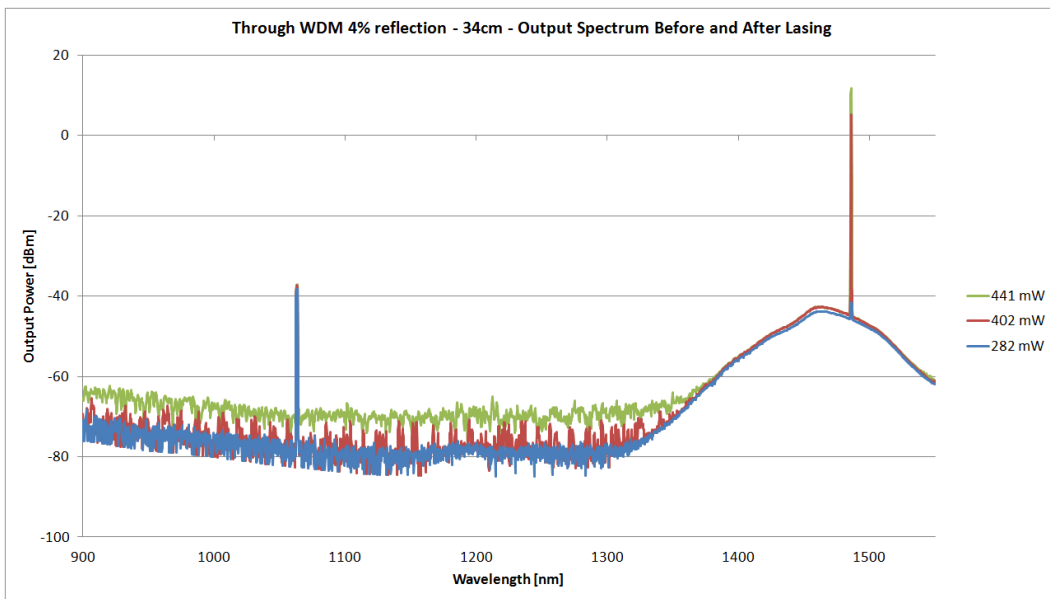


Figure 3.7: Spectrum of lasing at 1480 nm, using a 34 cm length of ZBLAN fiber

In the figure, we plot the curves of the spectrum before lasing begins (282 mW pump power - blue curve), at the threshold of lasing (402 mW pump power - red curve) and at a point after lasing has been established (441 mW pump power - green curve). We can see that the pump signal at 1064 nm is heavily suppressed by the stop-band of the WDM coupler. Additionally, we can see the lasing line occurring at 1487 nm (in the pass-band of the WDM coupler) and confirm that the laser is spectrally stable when increasing the pump power. Finally, we can see the amplified spontaneous emission (ASE) generated by the ZBLAN fiber around 1480 nm. The roll-off in the ASE is due to a

combination of the emission profile of the gain fiber as well as the pass-band profile of the WDM coupler.

To conclude this section, a summary of the results from all six configurations using all six gain lengths is shown in Tables 3.2 and 3.3.

Table 3.1: Summary of conversion efficiency for all six configurations using six different lengths of ZBLAN gain fiber

Conversion Efficiency [%]	34 cm	40 cm	52 cm	60 cm	85 cm	140 cm
Through WDM 4% Reflection	32.2	28.1	30.6	26.7	21.4	16.4
Through WDM 30% to loop	14.8	15.1	12	14.4	11.8	6.8
Through WDM 70% to loop	6.9	7.2	5.2	6.3	4.9	2.7
Through FBG 4% reflection	15.2	17.6	16.6	21.4	17.4	8.1
Through FBG 30% to loop	11.4	10.3	8.2	12.2	9.5	4.7
Through FBG 70% to loop	5.5	4.9	3.7	5.3	4.2	2.1

Table 3.2: Summary of threshold power for all six configurations using six different lengths of ZBLAN gain fiber

Threshold Power [mW]	34 cm	40 cm	52 cm	60 cm	85 cm	140 cm
Through WDM 4% Reflection	401.70	406.62	491	406.62	456.56	516.09
Through WDM 30% to loop	358	345.16	416	364.75	385.57	540.3
Through WDM 70% to loop	287	268.04	340	305.44	345.16	437.04
Through FBG 4% reflection	890	586.21	651	547.57	510.74	726.05
Through FBG 30% to loop	505	510.74	542	440.42	440.42	651.9
Through FBG 70% to loop	329	404.4	471	331.95	404.4	578.44

3.4 Conclusion

The goal of this chapter was to determine the optimum lasing configuration and optimum length of gain fiber for lasing around 1480 nm using the 8000 ppm Tm³⁺:ZBLAN fiber. Based on the results presented, the optimum configuration consists of pumping the gain fiber through the WDM coupler along with using the 4% Fresnel reflection to complete the cavity and serve as the output coupler. Although other configurations can

offer a lower threshold power, this configuration gives by far the highest conversion efficiency. The optimum length was found to be in the range of 30-50 cm. As previously mentioned, an exact comparison is difficult to achieve due to the varying insertion loss of each length of fiber. Instead, a range of optimum lengths is given. Pumping through the WDM coupler and using the 4% Fresnel reflection with a 34 cm length of Tm^{3+} :ZBLAN fiber, a maximum output power of 400 mW was achieved, with 33% slope efficiency. The threshold pump power for this configuration and gain length was 400 mW. A fiber laser with this performance could be useful for pumping an EDFA or for detecting liquid water by exploiting its nearby overtone absorption peak.

It is possible to improve the conversion efficiency by creating a monolithic cavity by writing the FBG directly in ZBLAN fiber. This would remove the loss involved in transitioning from the ZBLAN gain fiber to the silica FBG, and vice-versa. Additionally, using a lower doping concentration would reduce the significance of cross-relaxation processes, thereby increasing the efficiency. However, this would require significantly longer lengths of gain fiber. Finally, it has been shown in [22] that pumping at 1040 nm can lead to higher efficiency and maximum output power.

Chapter 4 Dual-Band Lasing at 810/1480 nm

4.1 Introduction

Single-wavelength fiber lasers, similar to the one presented in the previous section, have been well researched and most of the current work is on increasing the maximum output power by making more efficient, monolithic cavities. However, there is also considerable interest in building dual-wavelength and multi-wavelength fiber lasers, as the applications of such a source are numerous. They have uses in WDM communication, light imaging and ranging (LIDAR), and fiber optic sensing. Furthermore, they can be used for microwave generation and in high-resolution spectroscopy. In [39], an Erbium-doped fiber (EDF) is used to generate a dual-wavelength laser near 1554 nm, with a wavelength spacing of 27 pm. Through heterodyning, this is used to generate a 3.389 GHz microwave signal with a 3-dB linewidth of approximately 20 kHz. In [13], dual-wavelength detection is performed using cavity ring-down spectroscopy (CRDS). In this case, two diode lasers were multiplexed together to create the dual-wavelength source, however using a dual-wavelength fiber laser would provide a much more compact approach. This would also avoid the need for any additional wavelength multiplexing, as both wavelengths would be generated on a single fiber.

In section 2.4, there were many reports of dual-wavelength fiber lasers. However, in all of the examples described a dual-wavelength fiber laser where both lasing lines were located within the same spectral band (around 800 nm or around 1480 nm). A fiber laser emitting light in two different wavelength bands can potentially be even more useful. A much wider range of differential absorption measurements can be performed when using two wavelengths that are far apart. They can also be used in CRDS for detection at

very different wavelengths. Furthermore, in the biomedical field, a dual-band laser source can be employed in spectroscopic optical coherence tomography (SOCT) for rapid imaging of biological samples to classify different types of tissues [40].

In this section, a dual-band fiber laser operating simultaneously at 810 nm and 1480 nm is presented. To my knowledge, this is the first demonstration of a fiber laser using two different transitions starting from the same level, namely the ${}^3\text{H}_4 \rightarrow {}^3\text{H}_6$ and ${}^3\text{H}_4 \rightarrow {}^3\text{F}_4$ transitions, respectively (as shown in Fig. 4.1). In addition to the possible uses in CRDS and SOCT, these two wavelengths represent the first and third communication windows, respectively, and thus can be potentially used in WDM applications.

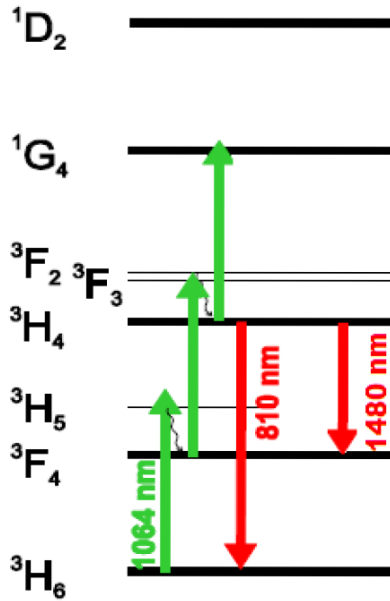


Figure 4.1: Upconversion pumping at 1064 nm to produce dual-band lasing at 810 nm and 1480 nm

4.2 Experimental Setup

The schematic for the dual-band laser cavity is shown in Fig. 4.2. The gain medium is the same Tm³⁺:ZBLAN fiber as in the previous section.

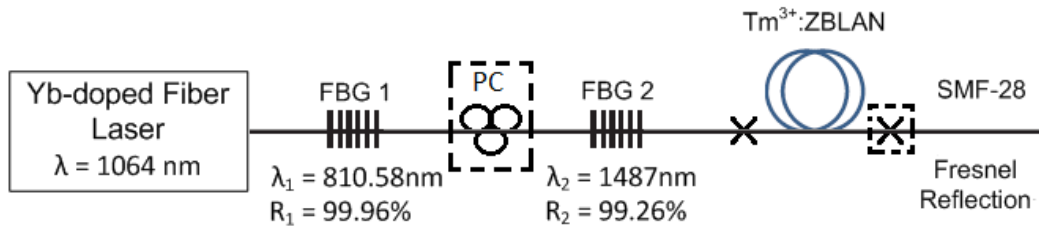


Figure 4.2: Dual-band fiber laser cavity. Dashed boxes represent that a measurement was done with and without the component.

Since we are still exciting the 3H_4 level, many of the pumping schemes shown in the previous section can be used here. Certain configurations will favour lasing at 1480 nm, while others will favour lasing at 810 nm. In this section, we again use up-conversion pumping at 1064 nm from an YDFL. We are forced to use linear cavities and pump through the FBGs as there is no WDM coupler that can pass the 1064 nm pump on one branch and the signals at 810 nm and 1480 nm on the other branch.

In Fig. 4.2, there are two cavities formed to realize the dual-wavelength operation. For lasing at 810 nm, the cavity is formed on one end by an FBG written in SM-780-HP fiber (FBG₁), which is optimized for single-mode operation at 800 nm. It has center wavelength $\lambda_1 = 810.58$ nm with a bandwidth $\Delta\lambda_1 = 0.2$ nm and peak reflectivity $R_1 = 99.96$ %. The cavity at 1480 nm is formed on one end by FBG₂ written in SMF-28 fiber, with center wavelength $\lambda_2 = 1487.03$ nm with a bandwidth $\Delta\lambda_2 = 0.4$ nm and peak reflectivity $R_2 = 99.26$ %. The two cavities both share a 4% Fresnel air reflection to form the other end of their respective cavities. Note that while the gain fiber is single mode at 1480 nm, it can support several modes at 800 nm.

FBG₁ was placed first in the setup as the SM-780-HP fiber is designed for low-loss operation around 800 nm and has very high loss at 1480 nm. Therefore, it was necessary to place it outside of the 1480 nm lasing cavity. However, this placement also helped in balancing the output power of the two signals. In Thulium, we expect a larger

gain at 810 nm as the emission cross section is much larger at this wavelength than at 1480 nm. By placing FBG₁ first, we partially compensate for this as it causes the cavity at 810 nm to include the insertion loss of FBG₂ (approximately 1 dB), while the cavity at 1480 nm has no additional losses.

The air gap used to create the 4% Fresnel air reflection is also used as the output coupler to an OSA (HP70952). A spectrum analyzer is necessary in this case in order to measure the power at each wavelength, rather than the total power. The air gap is created by placing two pigtails on two XYZ translation stages (i.e., capable of movement in 3 dimensions), as shown in Fig. 4.3.



Figure 4.3: Pigtails placed on XYZ translation stages

One pigtail is connected to the OSA, while the other pigtail is connected to the ZBLAN fiber. The translation stages, with the help of a microscope, are used to align the two fibers as closely as possible to minimize the loss, while avoiding contact in order to maintain an air gap. The distance between the two fibers is then increased along the fiber axis until a loss of 10 dB is created. This is done to reduce the power directed to the OSA, which has a limit of approximately 15 dBm. Since there is no WDM coupler to filter

out the pump source, the power levels would easily exceed this value without the additional attenuation. This artificial loss is taken into account and calibrated out when the results are reported.

Similar to the previous section, several different lengths of $\text{Tm}^{3+}:\text{ZBLAN}$ fiber were measured in order to evaluate the performance of the dual-band fiber laser as a function of gain length. In addition, as indicated by the dashed lines in Fig. 4.2, a set of measurements were performed with and without a polarization controller (PC) between the two FBGs. The PC adds an insertion loss of 0.5 dB to the cavity at 810 nm; however by partially separating the lasing lines to different polarization states, the competition between them can be reduced and the overall stability can be improved.

4.3 Experimental Results

As in the previous section, each configuration (with and without PC) was measured using six different sections of gain fiber: 34 cm, 40 cm, 52 cm, 60 cm, 85 cm, and 140 cm. From each measurement, we examine the fluctuations in the output power (i.e., the stability of the laser) as well as the threshold pump power for lasing at each wavelength. Since both transitions originate from the same energy level, we expect there to be competition between the two wavelengths. Measuring the output power fluctuations allows us to partially quantify this competition and to determine the optimum operating conditions for stability. Additionally, by looking at the threshold pump powers, we can determine the regions where the laser is operating at both wavelengths.

The pump power, P_{pump} , is taken as the output of the YDFL, i.e., the power just before FBG_1 in Fig. 4.2. It is measured independently by connecting the output of the YDFL to the OSA through the XYZ translation stage with the 10 dB loss (by

disconnecting the pigtail connected to the ZBLAN fiber). This was done to have a better comparison with the output power, which requires the use of an OSA to measure the power at λ_1 and λ_2 separately. As is the case with the output power measurement, the 10 dB loss is calibrated out when the pump power values are reported. Note that in this chapter, we are more concerned with the relative powers, i.e., the power at λ_1 compared with the power at λ_2 , as well as the output power vs. pump power. The absolute power values are not as significant in this chapter, and will be different than in the previous chapter as we are using an OSA rather than the Thorlabs power meter.

For each measurement, the results were obtained by sweeping the external current source from 1 A to 7 A, in steps of 0.2 A (which provides increments of 25 mW of pump power on average). At each step, six scans are taken on the OSA and the average power at λ_1 and λ_2 from the scans is extracted. The variation (standard deviation) observed during the six scans is represented by error bars on the plots. For the set of measurements using a PC, the polarization controller was set for the first length (34 cm) and was not changed for the other five lengths.

Again, the entire measurement is automated, with a GPIB connection controlling the current source (and thus the pump power) as well as triggering the OSA scans at every step. In this section, only the plots used to highlight the observations made will be shown. The remaining plots can be found in the appendix. The output power vs. pump power measurements without a PC for 52 cm and 140 cm are shown in Fig. 4.4 and Fig. 4.5.

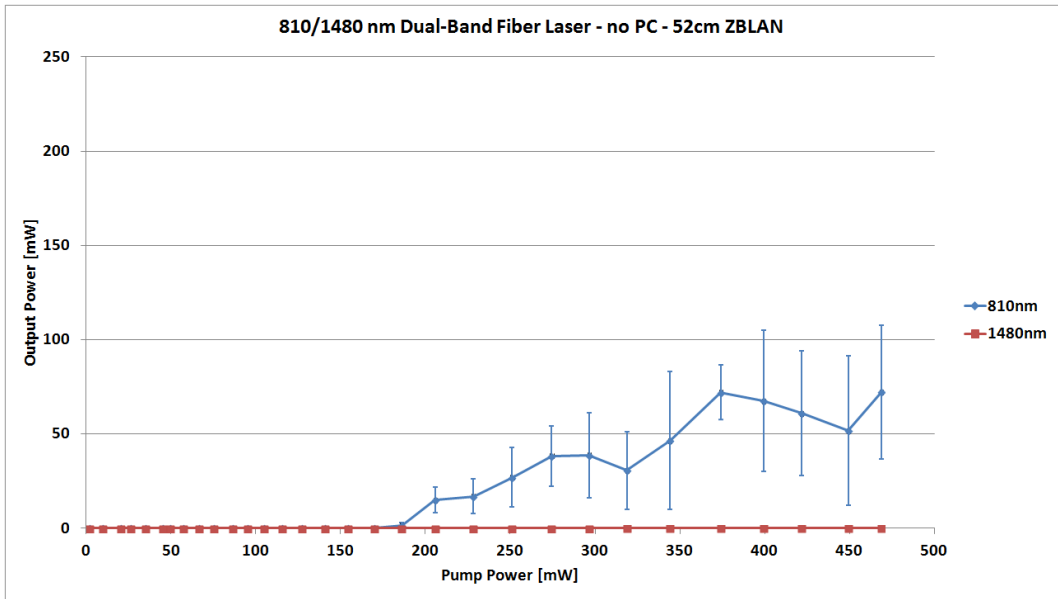


Figure 4.4: Output Power vs. Pump power without a PC for a 52cm Length of Gain Fiber

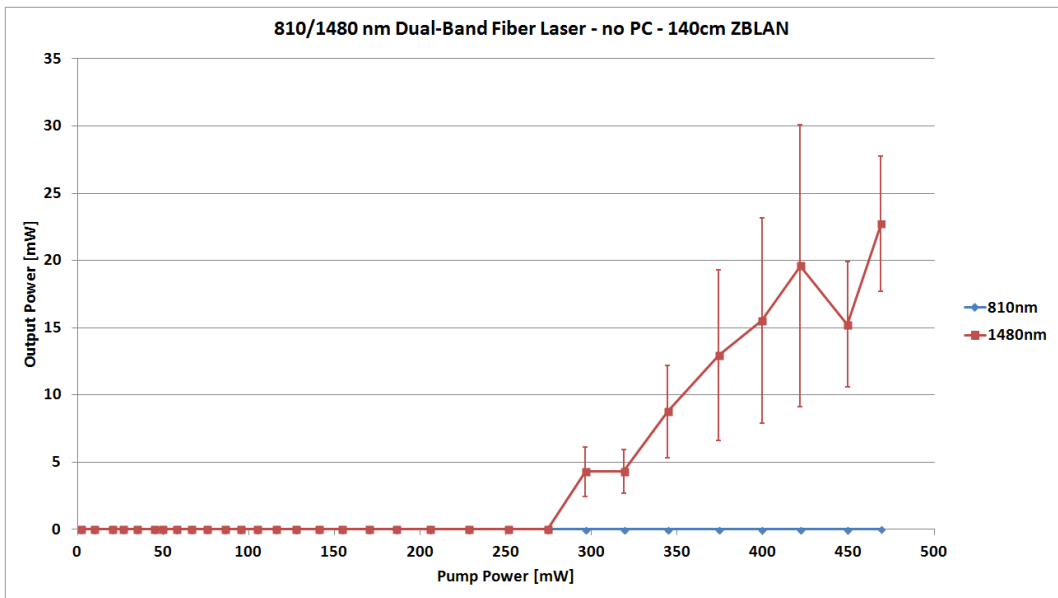


Figure 4.5: Output Power vs. Pump Power without a PC for a 140 cm Length of Gain Fiber

The blue curves represent the output power at λ_1 , while the red curves show the output power at λ_2 . As previously mentioned, the points on each curve represent the average of six OSA scans, while the error bars show the standard deviation of the six scans. From Fig. 4.4 and Fig. 4.5, we can see that without the use of a PC, dual-

wavelength operation is not always possible. Depending on the length of the gain fiber, one wavelength will dominate and can potentially suppress the other wavelength, preventing lasing. We can also see that increasing the length of the gain fiber favours operation at λ_2 , as with a 52 cm length the 1480 nm signal is completely suppressed, while with a 140 cm length the 810 nm signal is completely suppressed.

A second observation that can be made is that the variations in output power are smaller (i.e., more stable) in the regions where only one wavelength is lasing. A plot of the results from a 60 cm piece of Tm^{3+} :ZBLAN fiber with a PC is shown in Fig. 4.6. The threshold pump power for 810 nm is 125 mW, and for $125 \text{ mW} < P_{\text{pump}} < 250 \text{ mW}$ the average standard deviation of the output power is 9.35 and 8.34 for the signals at λ_1 and λ_2 , respectively.

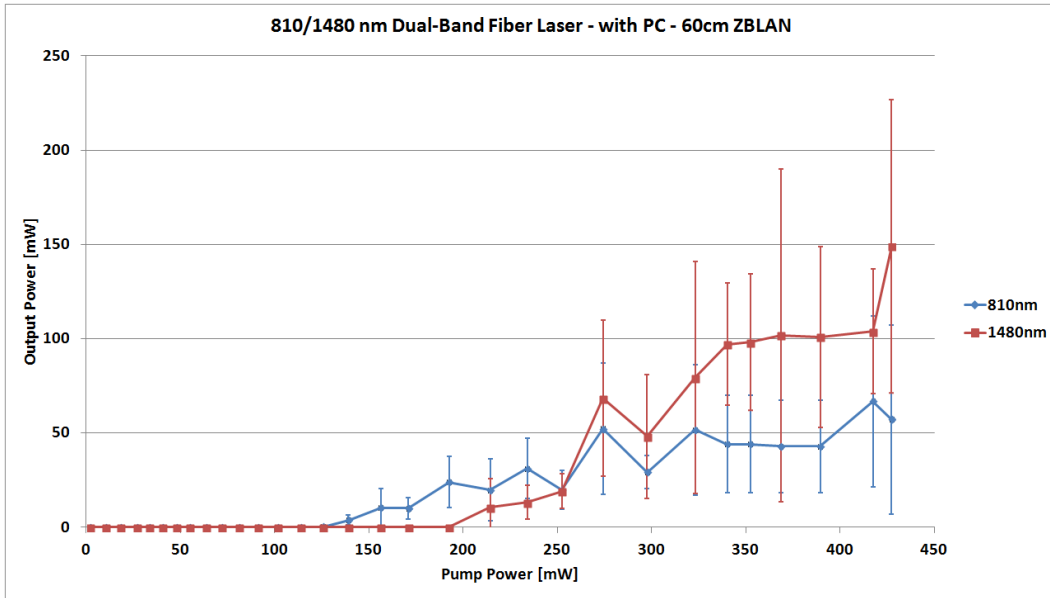


Figure 4.6: Output Power vs. Pump Power with a PC for a 60 cm Length of Gain Fiber

After 250 mW ($250 \text{ mW} < P_{\text{pump}} < 425 \text{ mW}$), both wavelengths have strong signals, giving an average standard deviation of 30.44 and 50.16 for the output power at

λ_1 and λ_2 , respectively. This increase in variation can be attributed to stronger competition between the two lasing lines.

Finally, we note that the optimum length for dual-wavelength operation is around 85 cm, as shown in Fig. 4.7. This is somewhat expected, as we saw from figures 4.4 and 4.5 that a gain length of 52 cm favours operation at λ_1 , while a gain length of 140 cm favours operation at λ_2 . We would therefore expect a length in the middle to be a good compromise between the two wavelengths. The optimum length is determined based on the ability to operate at λ_1 and λ_2 simultaneously with the minimum variation possible. Using this length, we see that the laser emits with roughly equal output powers at λ_1 and λ_2 , with an average slope efficiency of ~20%.

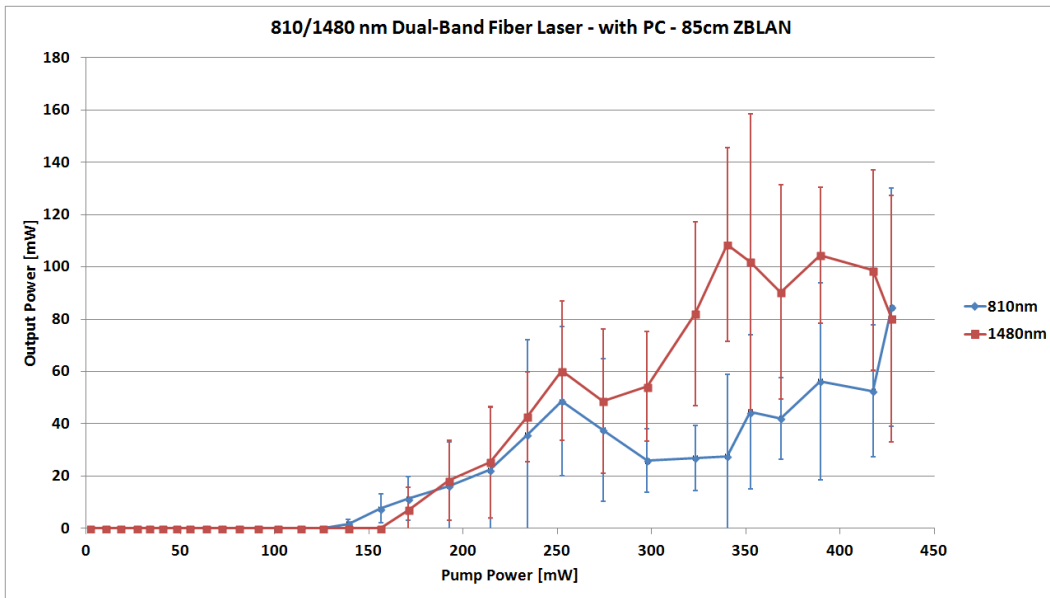


Figure 4.7: Output Power vs. Pump Power with a PC for an 85 cm Length of Gain Fiber

As in the previous section, for completeness a plot of the spectrum of dual-band fiber laser is shown in Fig. 4.8. We can see the peaks at the two laser wavelengths – i.e., around 810 nm and around 1480 nm. However, also present is a peak at the pump wavelength (1064 nm). We require high pump powers in order to reach the lasing

thresholds for the signals at 810/1480 nm. As a consequence some of this pump power leaks through to the output as there is no WDM coupler to filter this out. An additional small peak at 980 nm is also present and represents the pump for the YDFL.

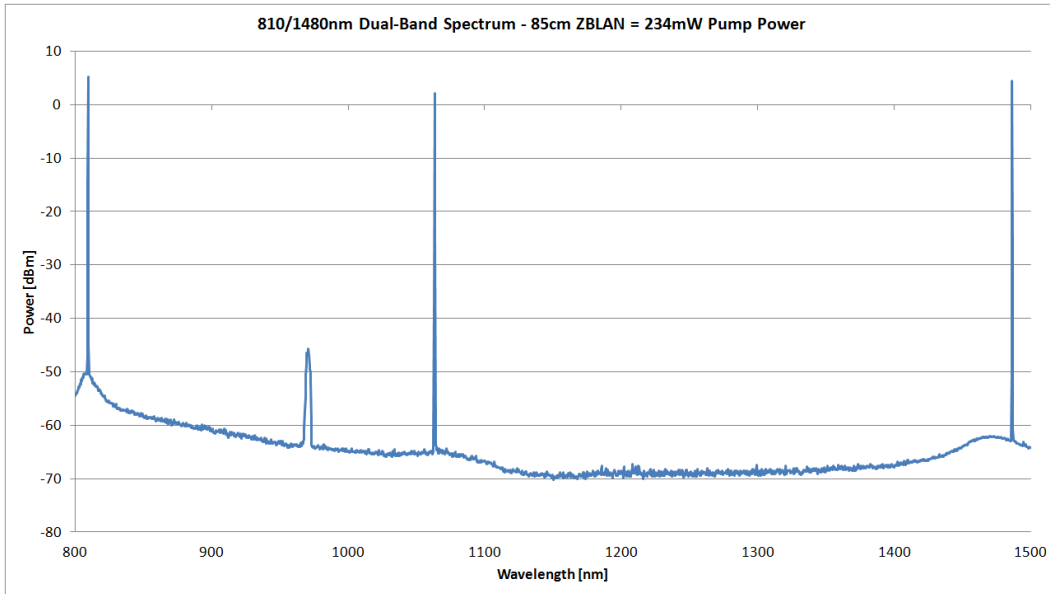


Figure 4.8: Output spectrum of dual-band fiber laser

4.4 Conclusion

The goal of this chapter was to investigate the dynamics involved with dual-wavelength lasing. To this end, dual-band lasing through two transitions which share the same upper laser level, namely the $^3H_4 \rightarrow ^3H_6$ transition (810 nm) and the $^3H_4 \rightarrow ^3F_4$ transition (1480 nm), was demonstrated. This was achieved using the configuration shown in Fig. 4.2. The optimum gain fiber length for simultaneous operation at 810 nm and 1480 nm was found to be around 85 cm of Tm^{3+} :ZBLAN fiber, as shorter lengths tended to favour operation at 810 nm, while longer lengths would favour operation at 1480 nm. A detailed numerical analysis would be required in order to determine the exact optimum fiber length. Roughly equal output power at the two laser wavelengths was obtained, with a ~20 % slope efficiency. Peak fluctuations in output power at relevant

points (i.e., at equal output power for both wavelengths) are within 1.5 dB. Output power stability is an important parameter if the laser is to be used for any practical application.

It is worth highlighting the importance of the polarization controller in achieving dual-band lasing. Without the PC, only a small range of gain fiber lengths would be capable of achieving dual-band lasing. However, by carefully tuning a PC placed inside the cavity, dual-band lasing can be achieved for a much larger range of gain fiber lengths. It also worth mentioning that temporal dynamics were not considered in this chapter.

Chapter 5 Triple-Wavelength Laser at 1460/1503/1873 nm

This chapter presents the experimental results obtained from a three-wavelength Tm³⁺:ZBLAN fiber laser operating at 1460 nm, 1503 nm and 1873 nm. The laser performance was fully characterized and was then used to measure the absorption of varying concentrations of water in acetone. Section 5.1 provides the motivation for creating a multi-wavelength laser at the given wavelengths. Section 5.2 describes the experimental setup used to create the three-wavelength laser, as well as the setup used for the absorption measurements. Section 5.3 presents the characterization of the laser performance and the results obtained from the absorption measurements. Section 5.4 concludes the chapter with a summary and a discussion on the results obtained.

5.1 Introduction

As was mentioned in the previous chapter, fiber lasers operating simultaneously at multiple wavelengths have numerous applications ranging from long-haul communication to chemistry to biology and medicine. Of particular interest in this chapter is the use of multi-wavelength fiber lasers for improving chemical detection. By emitting light simultaneously at different wavelengths with varying absorption levels, an absorption 'pattern' can be detected which can improve the specificity and sensitivity of the detection.

The near-infrared (NIR) region is particularly suitable for certain chemical detection problems. Most analytes show a structured overtone or combination band spectrum in the NIR that is as distinct as the corresponding mid-infrared (mid-IR) spectrum. Even though the transitions are weaker, the observed spectral response may

be similar due to the existence of strong laser light sources that can be spectrally tuned.

The absorption profile of liquid water is shown in Fig. 5.1.

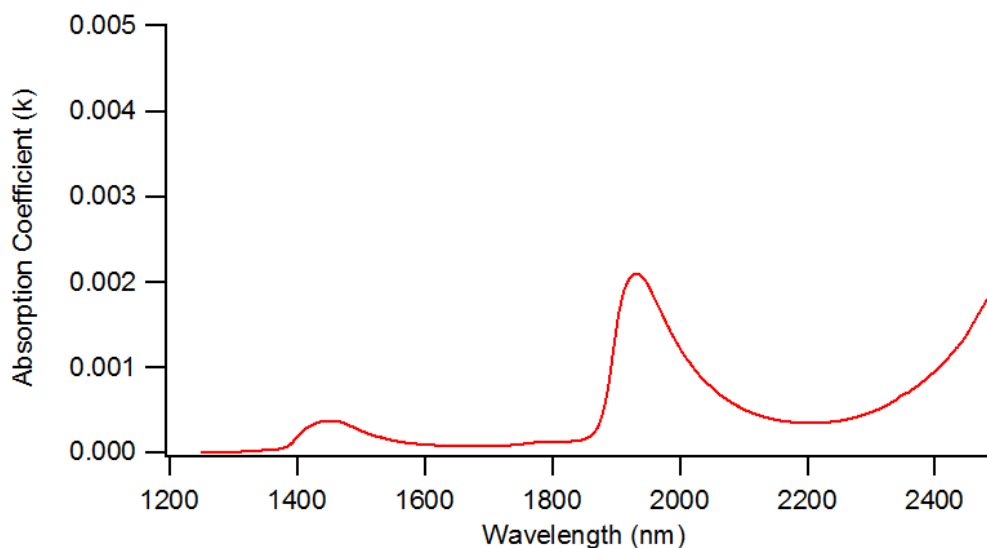


Figure 5.1: Near-Infrared Region Absorption Spectrum of Water [41]

The fiber laser was designed such that the peak wavelengths would fall at points with very different absorption coefficients. From Fig. 5.1, we can see that in liquid water, there exists two overtone absorption peaks in the NIR, one around 1480 nm and one around 1900 nm. Two of the wavelengths of the fiber laser were therefore placed near each of the absorption peaks, while the third was placed at a point of minimal absorption. To this end, we used the ${}^3\text{H}_4 \rightarrow {}^3\text{F}_4$ transition to generate lasing at 1460 nm (first local minima) and at 1503 nm (minimal absorption), and the ${}^3\text{F}_4 \rightarrow {}^3\text{H}_6$ transition to generate lasing at 1873 nm (second local maxima). This provided a fiber laser which emitted at three wavelengths, each with different absorption coefficient for water.

As described in Section 2.4, there have been many reports of multi-wavelength fiber lasers in both ZBLAN and in silica. However, in none of the previous reports were attempts made to apply the multi-wavelength functionality to the detection and quantification of chemicals. This chapter demonstrates the use of a fiber laser which

emits at three wavelengths in the NIR – 1460 nm, 1503 nm, and 1873 nm – for detecting water in acetone. This chemical system was chosen because acetone as a solvent has a well-defined background spectrum that is known to have little effect on the absorption of the solute. The goal was to first establish the chemical detection functionality of the multi-wavelength fiber laser before proceeding to more complex solvents such as oils and fuels. The same method used in detecting water in acetone can be carried over to other matrices.

5.2 Experimental Setup

5.2.1 Three-Wavelength Fiber Laser

A schematic of the laser design is shown in Fig. 5.2. It consists of two independent branches – one for generating lasing at 1460/1503 nm (top) and one for generating lasing at 1873 nm (bottom) – as well as a third shared branch which combines the two and serves as the output. The gain medium for operation at 1460 nm and 1503 nm is a 52 cm length of Tm³⁺:ZBLAN fiber, while the gain medium for operation at 1873 nm is an 85 cm length of Tm³⁺:ZBLAN fiber. The gain fiber in both cases is the same fiber that was investigated in the previous chapters.

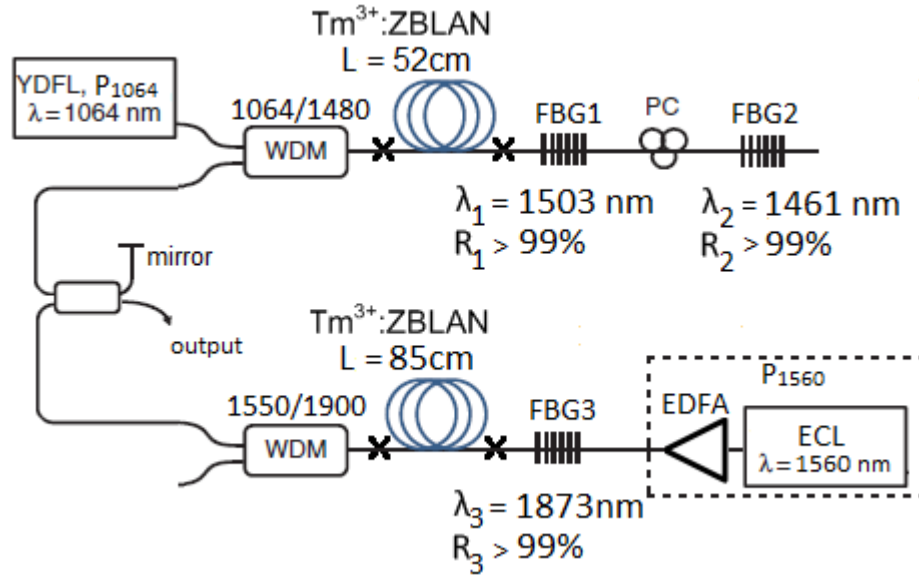


Figure 5.2: Tm³⁺:ZBLAN three-wavelength fiber laser configuration

The 52 cm length of gain fiber is pumped through a 1064/1480 WDM coupler by up-conversion pumping from a 1064 nm YDFL (P_{1064}), while the 85 cm length of gain fiber is pumped directly by a 1560 nm pump (P_{1560}) consisting of an external cavity laser (ECL) and an EDFA. The YDFL is again controlled by an external DC power supply. In the top branch, the cavity is formed on one end by two FBGs, which also define the lasing wavelengths. FBG₁ has center wavelength $\lambda_1 = 1503$ nm with $\Delta\lambda_1 = 0.15$ nm, while FBG₂ has center wavelength $\lambda_2 = 1461$ nm with $\Delta\lambda_2 = 0.486$ nm. In the bottom branch, the cavity is formed on one end by FBG₃, with center wavelength $\lambda_3 = 1873$ nm and $\Delta\lambda_3 = 0.3$ nm. All three gratings are written in SMF-28 fiber and have a peak reflectivity > 99%. The two branches are connected to a coupler and use a common gold-tipped fiber mirror on one of the coupler output ports to form the other end of their respective cavities. The fiber mirror has a reflectivity of approximately 90% at all laser wavelengths. The other port on the coupler serves as the output for all three wavelengths, and is connected to an OSA in order to measure the individual power at each wavelength. The coupler has a

50/50 splitting at 1460/1503 nm, while it has an 87/13 ratio at 1873 nm (87% to the mirror).

A PC is placed between FBG₁ and FBG₂ in order to balance the powers generated at λ_1 and λ_2 . By tuning the polarization controller, we can adjust the power at λ_2 such that it is similar to the power at λ_1 . This was necessary in order to ensure that lasing could occur simultaneously at both wavelengths; without the PC, the gain competition would allow only λ_2 to lase. As before, the Tm³⁺:ZBLAN gain fibers are coupled to the SMF-28 fibers through mechanical splices (represented by the 'x' in Fig. 5.2) which have a loss of 1.5-2.5 dB per pair.

5.2.2 Absorption Measurements

The three-wavelength laser shown in Fig. 5.2 was used to measure 12 samples with varying concentrations of water in acetone, ranging from 0.55 M to 11.4 M. A schematic of the setup used to perform single-pass absorption measurements on the samples is shown in Fig. 5.3.

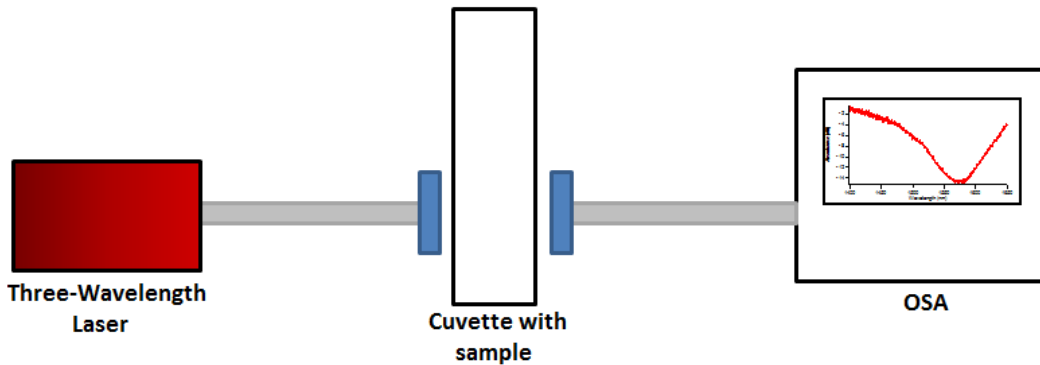


Figure 5.3: Experimental setup using three-wavelength laser for absorption measurements

The three-wavelength laser represents the output from Fig. 5.2 and the single-pass absorption measurements are done using an OSA in order to measure the absorption at each laser wavelength simultaneously. The sample was placed into a 1 cm quartz

cuvette and was coupled to the laser output using gradient-index (GRIN) lenses. The samples are tested in sequence by measuring the output power on the OSA and comparing it with a reference measurement obtained from a 100% acetone sample (0% water). The amount of power (in dB) absorbed by the sample is then calculated by subtracting the reference measurement from the sample measurement (for each wavelength).

For each sample, two reference measurements on the 100% acetone sample were taken: one before the sample measurement, and one after the sample measurement. This was to reduce the effect of any fluctuations in the laser output power. In addition, for each measurement, 30 scans from 1450 nm to 1900 nm were performed on the OSA (with a resolution bandwidth of 0.5 nm) and all the scans were averaged. This was done for both the sample measurement and reference measurement, and was to once again reduce the effect of any power fluctuations.

5.3 Experimental Results

5.3.1 Three-Wavelength Laser Characterization

The two branches of the three-wavelength laser are first characterized independently. To this end, the output power at λ_1 and λ_2 vs. P_{1064} are measured with $P_{1560} = 0$, and the output power at λ_3 vs. P_{1560} is measured with $P_{1064} = 0$. As before, these are done by increasing the pump powers in increments of 20-30 mW and measuring the output power at each wavelength on the OSA. P_{1064} represents the 1064 nm pump power, taken directly after the 1064/1480 WDM coupler, and P_{1560} represents the 1560 nm pump power and is taken after the EDFA.

Following this, we repeat the measurements with both pumps turned on to ensure that both branches are independent of each other. To this end, we set $P_{1560} = 500$ mW and measure the output power at λ_1 and λ_2 vs. P_{1064} , and set $P_{1064} = 1500$ mW and measure the output power at λ_3 vs. P_{1560} . The two set of measurements (with opposing pump turned on and off) are shown in Fig. 5.4 and 5.5, for λ_1/λ_2 and λ_3 , respectively.

In Fig. 5.4, we see that no lasing occurs until the first threshold pump power of 522 mW, when lasing begins at λ_2 . As the pump power is increased further, single-wavelength lasing at 1460 nm continues with 2.2% conversion efficiency up to a saturated output power of 15 mW. At this point, the second threshold pump power of 1144 mW is reached; lasing begins at λ_1 and continues with 3.4% conversion efficiency. The laser emits at both wavelengths (with a higher power at λ_2) until P_{1064} reaches around 1580 mW. At this point we observe approximately equal power at both wavelengths. As P_{1064} is increased to 1859 mW, the power at λ_1 increases to a maximum output of 21 mW, while the power at λ_2 keeps a saturated output of 15 mW. We also see that the curves are essentially the same regardless of whether P_{1560} is turned on or off. This demonstrates that the top branch is independent of the bottom branch.

In Fig. 5.5, we see that lasing at λ_3 begins at a threshold pump power of 126 mW and continues with a conversion efficiency of 2.5% as P_{1560} is increased. The output reaches a maximum of 13 mW at a pump power of 637 mW. Once again, we see that the curve is the same regardless of the state of P_{1064} , which shows that the bottom branch also operates independently of the top branch.

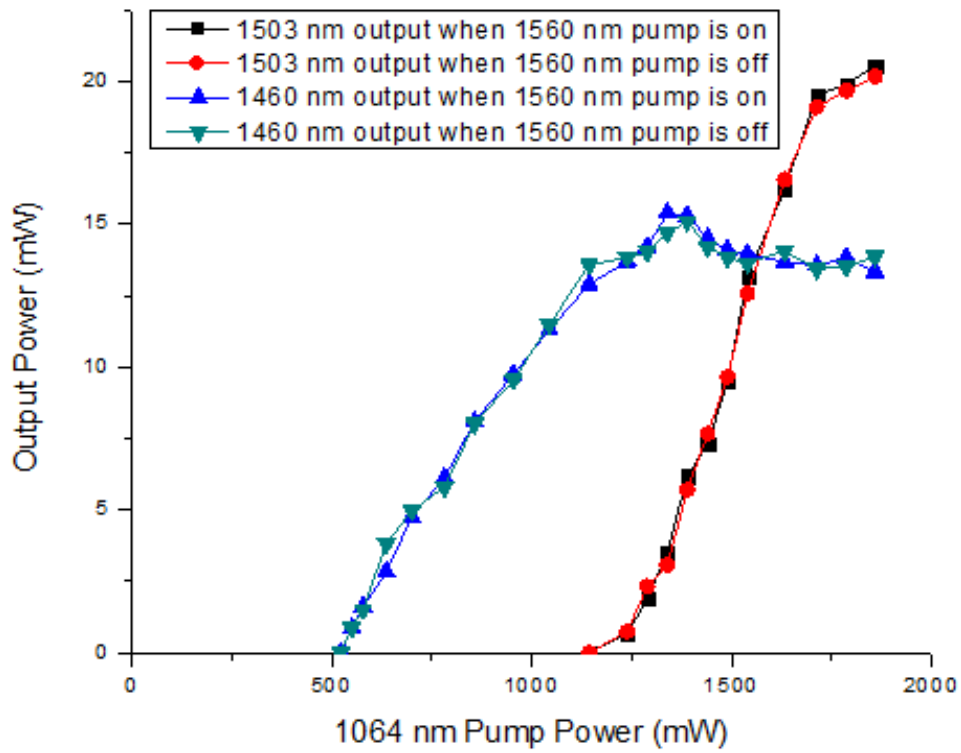


Figure 5.4: Output power at λ_1 and λ_2 vs. P_{1064} , with P_{1560} on and off

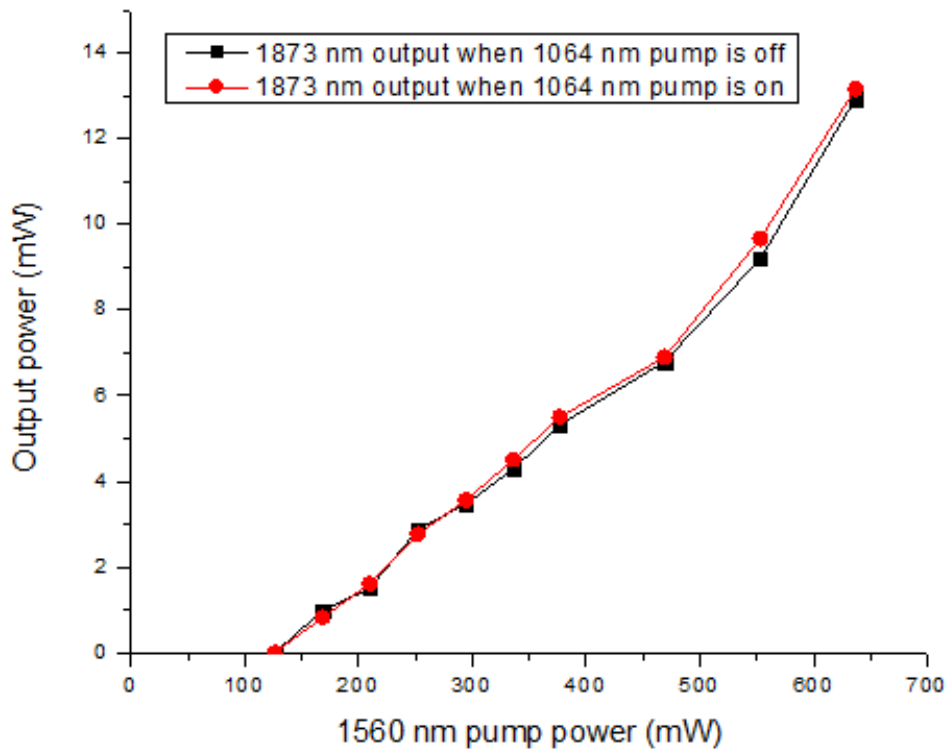


Figure 5.5: Output power at λ_3 vs. P_{1560} with P_{1064} on and off

For completeness, Fig. 5.6 shows the spectrum of the laser when all three-wavelengths are lasing. It was taken from the OSA for $P_{1064} = 1500$ mW and $P_{1560} = 500$ mW, which are also the pump powers used for the single-pass absorption measurements.

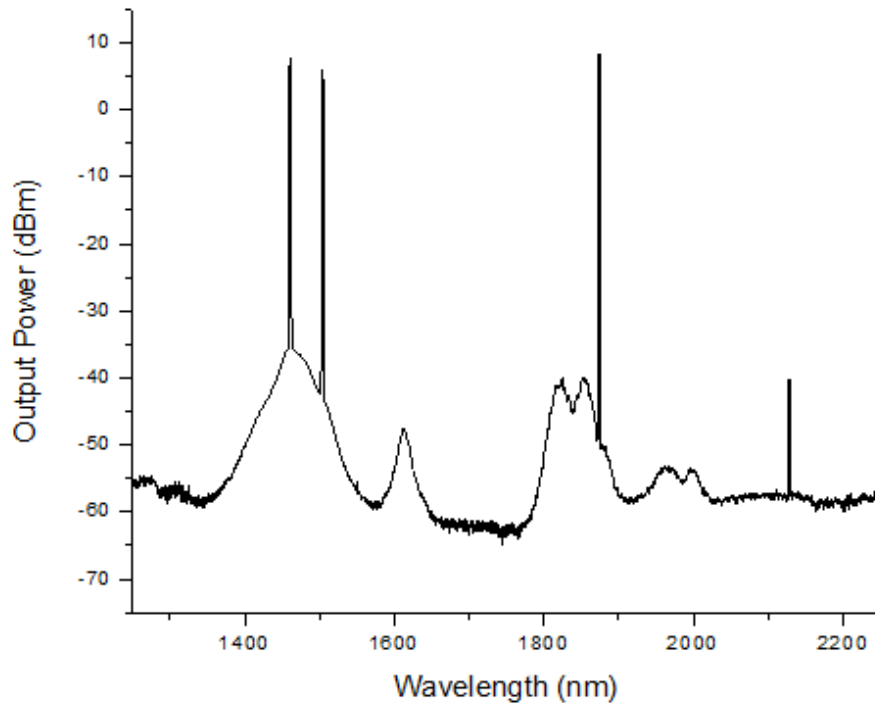


Figure 5.6: Output spectrum of the three-wavelength laser operation for $P_{1064} \sim 1500$ mW and $P_{1560} \sim 500$ mW

We can see the ASE created by the Tm^{3+} :ZBLAN fiber, as well as the three laser peaks at the FBG wavelengths, with peak powers all above 5 mW. Note that we see a small peak at 2128 nm, which is an artifact of the OSA due to higher-order diffraction from the P_{1064} .

To complete the characterization of the three-wavelength laser, we next examine the output power stability. This is a crucial metric for absorption measurements as it is very difficult to define a reference measurement if the power fluctuations are too large. To

this end, we set the pump powers as before ($P_{1064} = 1500 \text{ mW}$, $P_{1560} = 500 \text{ mW}$) and measure the power at each wavelength over a 30 minute period on the OSA. This is shown in Fig. 5.7. We can see that the peak power fluctuation for operation at λ_2 and λ_3 is about 1 dB, while the fluctuation at λ_1 is about 1.5 dB. These fluctuations are mainly due to mode competition in the cavity, as well as environmental variations.

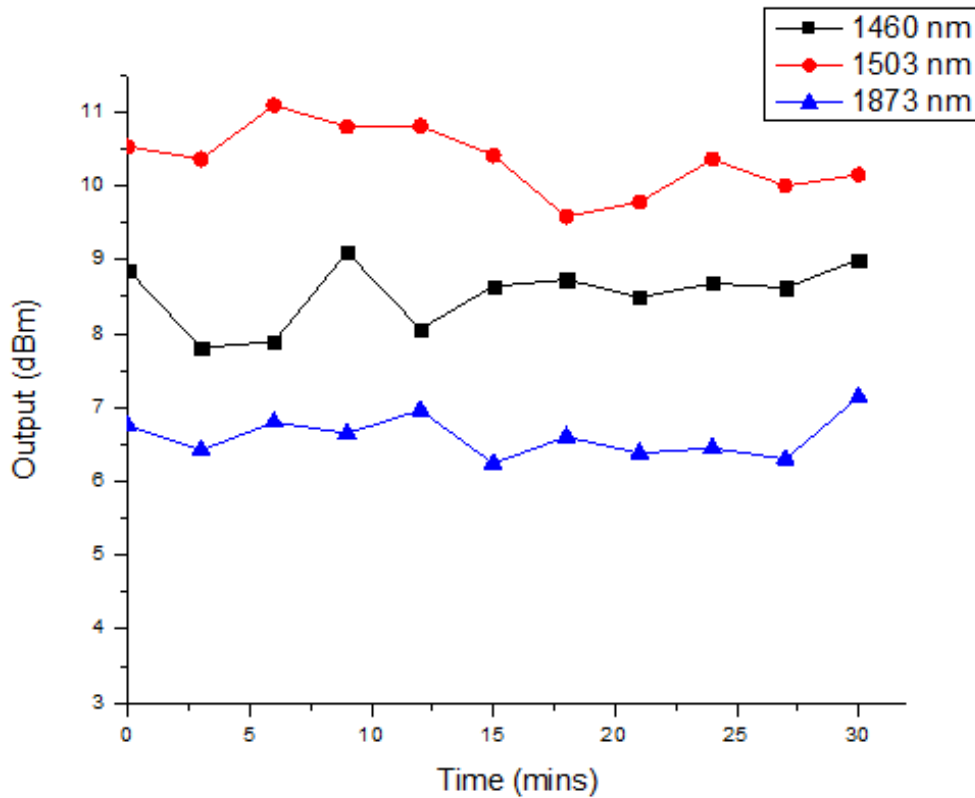


Figure 5.7: Output power fluctuations of three-wavelength laser with $P_{1064} = 1500 \text{ mW}$ and $P_{1560} = 500 \text{ mW}$

As an additional feature of the laser, we can look at the effect of the PC in the top branch. It was placed in the cavity to overcome the gain competition between the peaks at λ_1 and λ_2 in order to establish dual-wavelength operation. However, as a result, it can also be used to perform switching between single-wavelength operation at 1460 nm, single wavelength operation at 1503 nm, and 1460/1503 nm dual-wavelength operation. To demonstrate this, we set P_{1064} to 1.7 W and adjust the PC, as shown in Fig. 5.8.

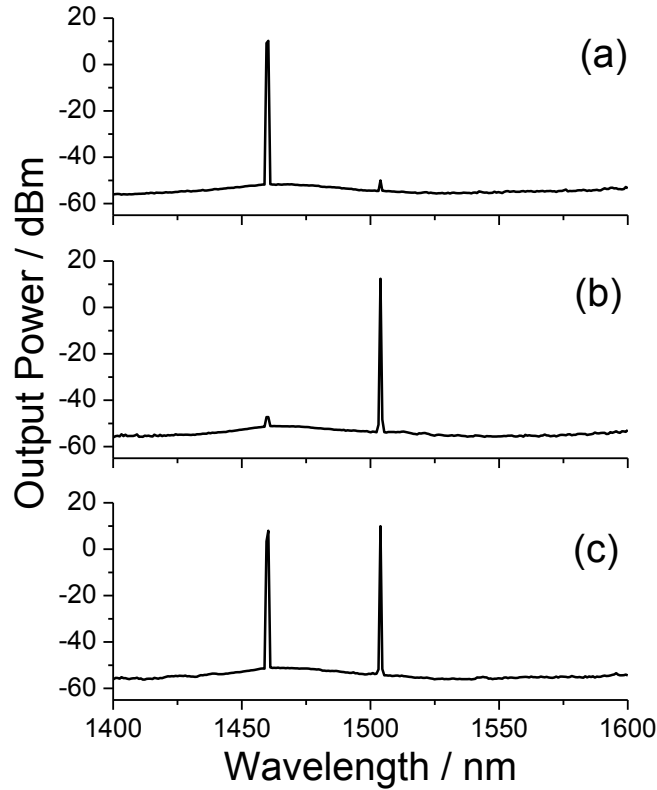


Figure 5.8: Output spectrum showing switching between (a) single-wavelength at λ_2 (b) single-wavelength at λ_1 (c) dual-wavelength at λ_1/λ_2 nm

5.3.2 Water in Acetone Absorption Measurements

The absorption measurements taken with the three-wavelength laser on the 12 samples of water in acetone are shown in Fig. 5.9. We can see that the absorption at each lasing wavelength as a function of water concentration shows approximately linear trends. The two blue lines represent the 99% confidence intervals, indicating the detection limits, as in [42]. The molar absorptivity, ϵ , can be calculated from the slope of each linear fit (red line). The lowest detection limit (about 2.8 M) is observed through the absorption curve at 1460 nm, presumably due to the larger absorption cross section and the more stable operation of the laser at this wavelength.

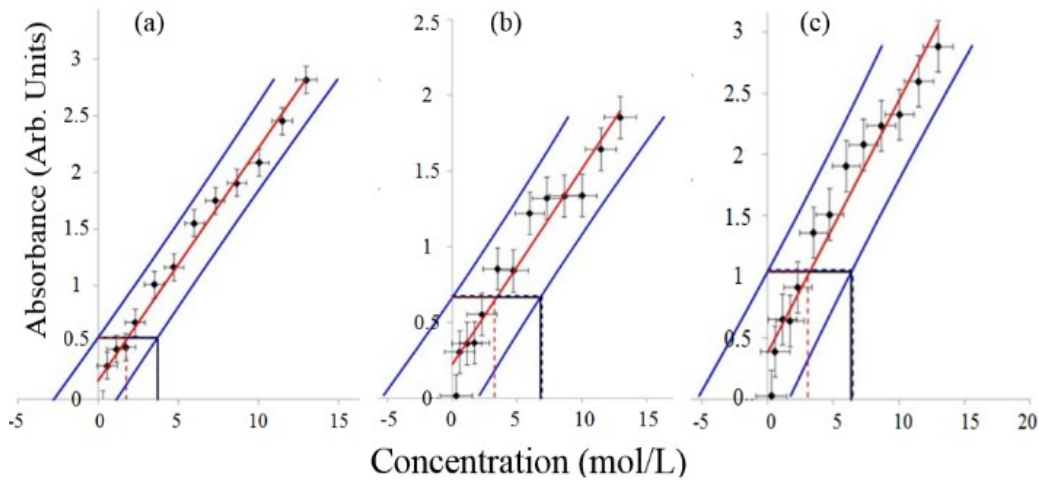


Figure 5.9: Absorption of water in acetone at (a) 1460 nm (b) 1503 nm (c) 1873 nm

The ϵ obtained from each individual λ are only 10-20% away from the theoretical values.

These are shown in table 5.1, where the ϵ are calculated as in [42].

Table 5.1: Molar Absorptivity coefficients in [$L \text{ mol}^{-1} \text{ m}^{-1}$] obtained from the single-pass absorption measurements vs. theoretical values

Wavelength	Calculated Value	Theoretical Value
1460 nm	22.4 ± 0.8	25.5
1503 nm	13.9 ± 1.1	16.3
1873 nm	22.2 ± 1.6	18.2

A deeper analysis considering solvatochromic effects (wavelength shifts of absorption profile due to concentration changes) at all three wavelengths would be required to provide ϵ values which are consistent with those in the literature.

5.4 Conclusion

The purpose of this chapter was to demonstrate a three-wavelength Thulium-doped ZBLAN fiber laser and show its use for detecting water in acetone. To this end, a configuration using two independent branches is constructed, one for generating lasing at

1460 nm and 1503 nm through the ${}^3\text{H}_4 \rightarrow {}^3\text{F}_4$ transition, and one for generating lasing at 1873 nm through the ${}^3\text{F}_4 \rightarrow {}^3\text{H}_6$ transition. A 52 cm length of $\text{Tm}^{3+}:\text{ZBLAN}$ fiber is used for operation at 1460/1503 nm and an 85 cm length of $\text{Tm}^{3+}:\text{ZBLAN}$ fiber is used for operation at 1873 nm. Simultaneous emission at all three wavelengths with output powers above 5 mW is obtained, and the laser is shown to be stable by observing peak fluctuations within 1 dB at 1460/1873 nm, and within 1.5 dB at 1503 nm.

The three-wavelength laser is then used for single-pass absorption measurements on samples of water in acetone. A detection limit of 2.8 M is obtained, with molar absorptivity values within 10-20% of the theoretical values. This method can be easily extended to the detection of impurities in more relevant solvents, such as water in lubricant oils or water in hydrocarbon fuel, as the laser wavelengths can be easily tailored to match the profile of the solvent (by simply changing the FBG center wavelengths).

Chapter 6 Conclusion and Future Work

This thesis has presented the design and implementation of single, dual- and multi-wavelength Tm^{3+} :ZBLAN fiber lasers, operating at a wide range of wavelengths.

Chapter 2 presented a background on rare-earth doped fiber lasers, along with an investigation into the transitions of Thulium ions. Examples of how the different electron transitions of Tm^{3+} ions are used for lasing in both silica and ZBLAN were given, along with the differences between each glass host. Finally, the chapter concludes with a review of relevant multi-wavelength Tm^{3+} :ZBLAN fiber lasers. Similar investigations into other rare-earth elements (e.g. Erbium) are given in Appendix A.

Chapter 3 presented the design of an optimized laser cavity for operation around 1480 nm. Possible pumping schemes are discussed, along with a detailed review of up-conversion pumping configurations. The goal of this chapter was to determine the optimum laser configuration and gain fiber length. Details about the experimental setup for the different cavities are given, followed by the experimental results (threshold pump power, conversion efficiency, maximum output power) for each cavity/gain fiber length combination. It was determined experimentally that the optimum performance is obtained by using a 4% Fresnel air reflection at the output end of the cavity (instead of a loop mirror) along with a 30-45 cm length of Tm^{3+} :ZBLAN fiber. Using this, 32% conversion efficiency was obtained, with a maximum output power around 400 mW and a threshold pump power also around 400 mW. The performance could be improved by using a monolithic cavity (i.e., writing the FBGs directly in ZBLAN fiber) which would reduce the cavity loss significantly. Additionally, an improved process for splicing SMF-28 fiber to ZBLAN fiber would further reduce the cavity loss.

Chapter 4 presented the design of a dual-band Tm^{3+} :ZBLAN fiber laser operating at 810 nm and 1480 nm through the ${}^3\text{H}_4 \rightarrow {}^3\text{H}_6$ and ${}^3\text{H}_4 \rightarrow {}^3\text{F}_4$ transitions, respectively. This was the first demonstration of a fiber laser using two lasing transitions which originated from the same upper energy level (${}^3\text{H}_4$ in this case). It is made possible due to the extended lifetime of the ${}^3\text{H}_4$ state in ZBLAN glass (almost 10 times longer than in silica). It was found that shorter lengths favoured operation at 810 nm, while longer lengths favoured operation at 1480 nm. Furthermore, careful adjusting of a polarization controller was required to ensure dual-wavelength operation at a wide range of gain fiber lengths; measurements made without the PC showed that only certain lengths would support dual-wavelength operation. The optimum length was determined to be between 60-85 cm which provided simultaneous operation at both wavelengths with roughly equal output powers, 20% slope efficiencies and peak fluctuations within 1.5 dB. As before, FBGs writing directly in ZBLAN fiber, along with more efficient ZBLAN-SMF splicing would improve the performance.

Chapter 5 presents the design of a three-wavelength Tm^{3+} :ZBLAN fiber laser, emitting simultaneously at 1460/1503/1873 nm, and its use in detecting water in acetone. The fiber laser uses the ${}^3\text{H}_4 \rightarrow {}^3\text{F}_4$ transition for the 1460/1503 nm lasing lines, and the ${}^3\text{F}_4 \rightarrow {}^3\text{H}_6$ transition for the lasing line at 1873 nm. These lines were chosen to provide three wavelengths in the NIR with very different absorption coefficients in water, which allowed the detection of an absorption 'pattern'. The laser was first fully characterized, and was found to provide roughly 10 mW simultaneously at all three laser wavelengths. The peak fluctuations were stable within 1.5 dB. The fiber laser was then used for single-pass measurements on varying concentrations of water in acetone. The measurements obtained from each individual wavelength provided molar absorptivities

that were within 10-20% of the theoretical values. An analysis considering the solvatochromic effects at all three wavelengths could provide even more accurate results.

It is clear from chapters 3 and 4 that a detailed numerical model is required in order to fully optimize the cavity and gain fiber parameters. Future work in this area would be to create a detailed numerical simulation which would simultaneously solve the population equations and the propagation equations involved in the fiber lasers. This would need to account for stimulated emission and absorption, radiative and non-radiative decays, as well as cross-relaxation effects. With this, the exact gain fiber length and FBG reflectivities could be chosen to optimize the laser output. Another way to optimize the laser efficiency would be to reduce the cavity loss by implementing ZBLAN-SMF splicing. Currently, the two fibers are spliced together mechanically, with an insertion loss of about 2.5 dB per pair of splices. Using a Vytran fusion splicer, this loss could be reduced to about 0.75 dB per splice (or 1.5 dB per pair).

Regarding chapter 5, although the molar absorptivities obtained from each wavelength were within 10-20 % of theoretical values, the real benefit of using a multi-wavelength laser comes from a solvatochromic analysis. This accounts for the wavelength shifts of the absorption profile due to concentration changes by measuring the absorption at different points and detecting a 'profile'. This method looks promising for obtaining molar absorptivities which are very consistent with the literature. Finally, although the measurement was performed on water in acetone, the real value would come from measuring water in more useful solvents, such as gasoline or jet fuel. However, this same process could be easily extended to these solvents, and the laser wavelengths can be easily tailored as required by simply changing the FBG center wavelengths.

Appendix A

Erbium

The electronic transition diagram for Er^{3+} ions is shown in Fig. A.1. As previously mentioned, Erbium-doped fibers are critical for modern day optical fiber communications as they can provide amplification around 1550 nm, which is the center of the third telecommunication window. EDFAs use the $^4I_{13/2} \rightarrow ^4I_{15/2}$ transition for this purpose. Silica is a suitable glass host for this transition, as the lifetime of the $^4I_{13/2}$ state in silica is quite long (~10 ms). As was the case with Thulium, rather than directly pumping the $^4I_{13/2}$ level (with a 510 nm pump), it is more efficient to excite electrons to the $^4I_{11/2}$ level and allow them to rapidly decay to the $^4I_{13/2}$ level.

In a fluoride host, the $^4I_{11/2} \rightarrow ^4I_{13/2}$ transition producing light at 2700 nm is of particular interest. This wavelength is very close to the absorption peak of water (3000 nm) and thus a laser created through this transition can be used for many spectroscopic measurements. The $^4I_{11/2} \rightarrow ^4I_{13/2}$ transition is generally self-terminating, as the lifetime of the upper energy state (6.9 ms) is shorter than the lifetime of the lower energy state (9 ms) [25]. However, significant investigations into methods of alleviating this issue have been performed and in [26], a 24 W $\text{Er}^{3+}:\text{ZBLAN}$ fiber laser was demonstrated through diode-pumping at 975 nm.

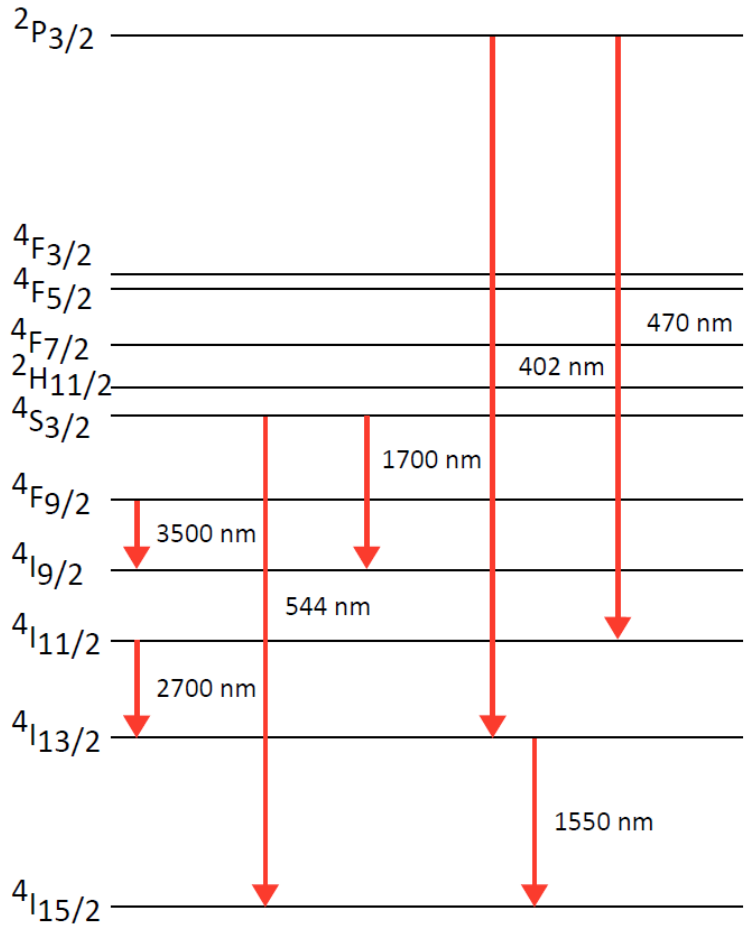


Figure 6: Electronic Transition Diagram of Er³⁺ Ions [6]

Neodymium

The electronic transition diagram for Nd³⁺ ions is shown in Fig. A.2. It was mentioned in the previous chapter that the first demonstration of a fiber laser was done using a Neodymium-doped silica fiber. Also noteworthy is that the first fiber laser developed in ZBLAN glass was also doped with Nd³⁺ ions [27]. The three main lasing transitions in Nd³⁺ ions are: $4F_{3/2} \rightarrow 4I_{9/2}$ (950 nm), $4F_{3/2} \rightarrow 4I_{11/2}$ (1100 nm) and $4F_{3/2} \rightarrow 4I_{13/2}$ (1300 nm). The $4F_{3/2} \rightarrow 4I_{13/2}$ transition has the strongest emission, and thus it is difficult to achieve lasing from the other two transitions due to gain competition. The $4F_{3/2}$ level can be populated by either pumping at 870 nm, or through the $4F_{5/2}/2H_{9/2}$ level by pumping at 800 nm.

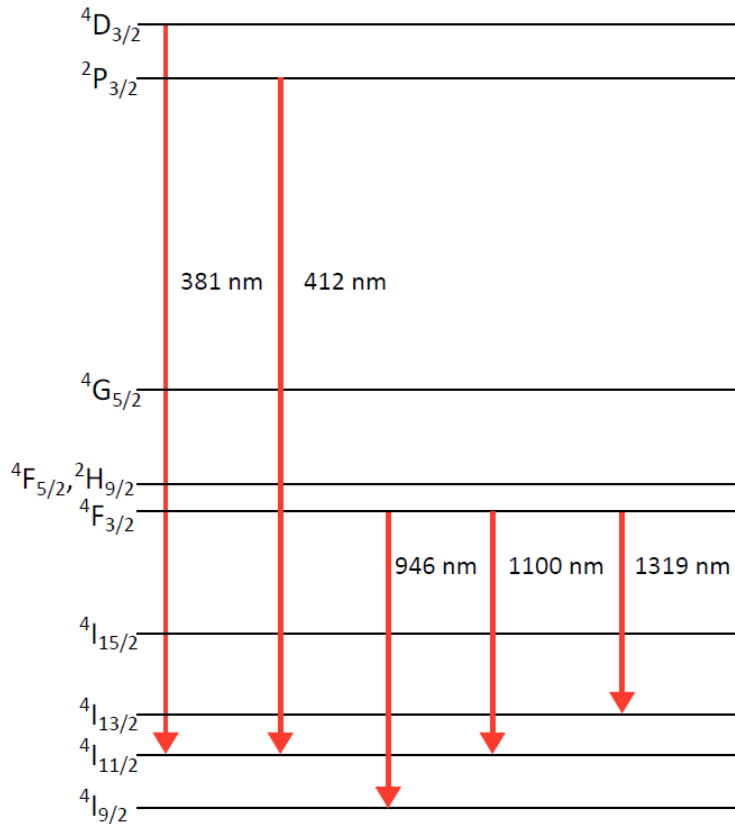


Figure A.2: Electronic Transition Diagram of Nd³⁺ Ions [6]

Ytterbium

The electronic configuration of Yb³⁺ ions is [Xe] 4f¹³. They are missing only one electron to fill the 4f shell, and thus their electronic transition diagram is very limited, as shown in Fig. A.3. The ²F_{5/2} level is populated by pumping around 940 nm, and the ²F_{5/2} → ²F_{7/2} transition emits light around 1050 nm. Ytterbium ions have very high quantum efficiency, and thus very high output powers can be obtained using Ytterbium-doped fiber lasers. Indeed, 1064 nm Ytterbium-doped fiber lasers are very commonly used for pumping Tm³⁺ ions.

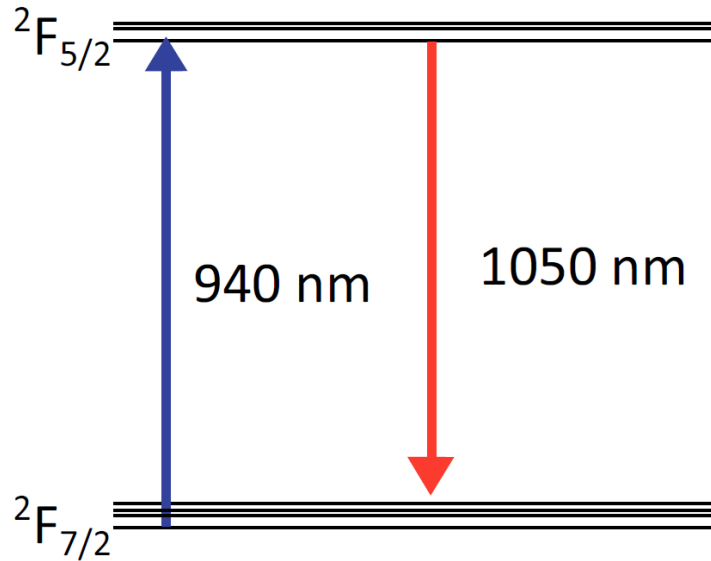


Figure A.3: Electronic Transition Diagram of Yb³⁺ Ions

1. Engineering, E. *Laser / Types and Components of Laser*. [cited 2014; Available from: <http://www.electrical4u.com/laser-types-and-components-of-laser/>].
2. Snitzer, E., *Proposed Fiber Cavities for Optical Masers*. *Journal of Applied Physics*, 1961. **32**(1): p. 36-39.
3. Mears, R.J., et al., *Neodymium-doped silica single-mode fibre lasers*. *Electronics Letters*, 1985. **21**(17): p. 738-740.
4. Langner, A., et al. *New developments in high power fiber lasers based on alternative materials*. 2011.
5. Latham, P. *Module 8 Laser/Fiber-Optic Communication Systems*. [cited 2014; Available from: <http://pe2bz.philpem.me.uk/Lights/-%20Laser/Info-999-LaserCourse/C00-M08-Laser-FiberOptic-CommunicationSystems/module8.htm>].
6. Frison, B., *Single and Dual-Wavelength Lasing in the 800-820 nm and 1460-1520 nm Bands in a Tm:ZBLAN Fibre Laser*, in *Department of Electrical and Computer Engineering*. 2013, McGill University: Montreal, Canada. p. 132.

7. Poulain, M., M. Poulain, and J. Lucas, *Verres fluores au tetrafluorure de zirconium proprietes optiques d'un verre dope au Nd³⁺*. Materials Research Bulletin, 1975. **10**(4): p. 243-246.
8. Lu, H.-y., *Development of ZBLAN Fiber-Based Components*. 2012, McGill University (Canada): Ann Arbor. p. 93.
9. Brilland, L., et al. *Development of highly nonlinear single mode chalcogenide microstructured optical fiber for Brillouin fiber laser applications*. in *Workshop on Specialty Optical Fibers and their Applications*. 2013. Sigtuna: Optical Society of America.
10. Wang, J.S., E.M. Vogel, and E. Snitzer, *Tellurite glass: a new candidate for fiber devices*. Optical Materials, 1994. **3**(3): p. 187-203.
11. Richards, B., et al. *1.91-1.99 um Tm³⁺/Yb³⁺ co-doped tellurite fibre laser pumped using a 1088 nm Yb³⁺ fibre laser*. in *Lasers and Electro-Optics, 2007 and the International Quantum Electronics Conference. CLEOE-IQEC 2007. European Conference on*. 2007.
12. Willer, U., et al., *Near- and mid-infrared laser monitoring of industrial processes, environment and security applications*. Optics and Lasers in Engineering, 2006. **44**(7): p. 699-710.
13. Waechter, H., et al., *Simultaneous and Continuous Multiple Wavelength Absorption Spectroscopy on Nanoliter Volumes Based on Frequency-Division Multiplexing Fiber-Loop Cavity Ring-Down Spectroscopy*. Analytical Chemistry, 2011. **83**(7): p. 2719-2725.
14. Xia, C., *Mid-infrared supercontinuum laser system and its biomedical applications*. 2009, University of Michigan: Ann Arbor. p. 160.
15. Laperle, P., *Etude de lasers a fibre emettant a 480 nm et du phenomene de coloration dans la fibre de ZBLAN dopee au thulium*. 2003, Universite Laval (Canada): Ann Arbor. p. 297-297 p.
16. Simakov, N., et al., *A cladding-pumped, tunable holmium doped fiber laser*. Optics Express, 2013. **21**(23): p. 28415-28422.
17. Walsh, B.M. and N.P. Barnes, *Comparison of Tm:ZBLAN and Tm:silica fiber lasers; Spectroscopy and tunable pulsed laser operation around 1.9 μm*. Applied Physics B, 2004. **78**(3-4): p. 325-333.
18. Eichhorn, M. and S.D. Jackson, *Comparative study of continuous wave Tm³⁺-doped silica and fluoride fiber lasers*. Applied Physics B, 2008. **90**(1): p. 35-41.
19. Zhu, X. and N. Peyghambarian, *High-Power ZBLAN Glass Fiber Lasers: Review and Prospect*. Advances in OptoElectronics, 2010. **2010**.

20. Layne, C.B., W.H. Lowdermilk, and M.J. Weber, *Multiphonon relaxation of rare-earth ions in oxide glasses*. Physical Review B, 1977. **16**(1): p. 10-20.
21. El-Agmy, R.M. and N.M. Al-Hosiny, *2.31 μm laser under up-conversion pumping at 1.064 μm in Tm^{3+} :ZBLAN fibre lasers*. Electronics Letters, 2010. **46**(13): p. 936-937.
22. Androz, G., et al., *2.3 W single transverse mode thulium-doped ZBLAN fiber laser at 1480 nm*. Optics Express, 2008. **16**(20): p. 16019-16031.
23. Allain, J.Y., M. Monerie, and H. Poignant, *Tunable CW lasing around 0.82, 1.48, 1.88 and 2.35 μm in thulium-doped fluorozirconate fibre*. Electronics Letters, 1989. **25**(24): p. 1660-1662.
24. Dennis, M.L., J.W. Dixon, and I. Aggarwal, *High power upconversion lasing at 810 nm, in Tm :ZBLAN fibre*. Electronics Letters, 1994. **30**(2): p. 136-137.
25. Peterka, P., et al., *Theoretical modeling of fiber laser at 810 nm based on thulium-doped silica fibers with enhanced 3H_4 level lifetime*. Optics Express, 2011. **19**(3): p. 2773-2781.
26. McCumber, D.E., *Einstein Relations Connecting Broadband Emission and Absorption Spectra*. Physical Review, 1964. **136**(4A): p. 954-957.
27. Androz, G., et al., *Self-pulsing dynamics of a dual-wavelength Tm^{3+} :ZBLAN upconversion fiber laser emitting around 800 nm*. Journal of the Optical Society of America B, 2007. **24**(11): p. 2907-2913.
28. Guanshi, Q., et al., *Multiple-wavelength up-conversion laser in Tm^{3+} -doped ZBLAN glass fiber*. Photonics Technology Letters, IEEE, 2005. **17**(9): p. 1818-1820.
29. Qin, G., et al., *784-nm amplified spontaneous emission from Tm^{3+} -doped fluoride glass fiber pumped by an 1120-nm fiber laser*. Optics Letters, 2005. **30**(3): p. 269-271.
30. Frison, B., et al. *Dual-wavelength lasing around 800 nm in a Tm :ZBLAN fibre laser*. in *Photonics Conference (IPC), 2012 IEEE*. 2012.
31. Frison, B., et al., *Dual-wavelength S-band Tm^{3+} :ZBLAN fibre laser with 0.6 nm wavelength spacing*. Electronics Letters, 2013. **49**(1): p. 60-62.
32. Allen, R., L. Esterowitz, and I. Aggarwal, *An efficient 1.46 μm thulium fiber laser via a cascade process*. Quantum Electronics, IEEE Journal of, 1993. **29**(2): p. 303-306.
33. Komukai, T., et al., *Upconversion pumped thulium-doped fluoride fiber amplifier and laser operating at 1.47 μm* . Quantum Electronics, IEEE Journal of, 1995. **31**(11): p. 1880-1889.

34. Kasamatsu, T., Y. Yano, and H. Sekita, *1.50-um-band gain-shifted thulium-doped fiber amplifier with 1.05- and 1.56-um dual-wavelength pumping*. Optics Letters, 1999. **24**(23): p. 1684-1686.
35. Cole, B. and M.L. Dennis. *S-band amplification in a thulium doped silicate fiber*. in *Optical Fiber Communication Conference and Exhibit, 2001. OFC 2001*. 2001.
36. Gomes, A.S.L., et al., *Characterization of efficient dual-wavelength (1050 + 800 nm) pumping scheme for thulium-doped fiber amplifiers*. Photonics Technology Letters, IEEE, 2003. **15**(2): p. 200-202.
37. Kasamatsu, T., Y. Yano, and T. Ono, *Laser-diode-pumped highly efficient gain-shifted thulium-doped fiber amplifier operating in the 1480-1510-nm band*. Photonics Technology Letters, IEEE, 2001. **13**(5): p. 433-435.
38. Roy, F., et al., *Noise and gain band management of thulium-doped fiber amplifier with dual-wavelength pumping schemes*. Photonics Technology Letters, IEEE, 2001. **13**(8): p. 788-790.
39. Yu, Y., et al., *Dual-wavelength erbium-doped fiber laser with a simple linear cavity and its application in microwave generation*. Photonics Technology Letters, IEEE, 2006. **18**(1): p. 187-189.
40. Zhu, R., et al., *Dual-Band Time-Multiplexing Swept-Source Optical Coherence Tomography Based on Optical Parametric Amplification*. Selected Topics in Quantum Electronics, IEEE Journal of, 2012. **18**(4): p. 1287-1292.
41. Bertie, J.E. and Z. Lan, *Liquid Water-Acetonitrile Mixtures at 25 °C: The Hydrogen-Bonded Structure Studied through Infrared Absolute Integrated Absorption Intensities*. The Journal of Physical Chemistry B, 1997. **101**(20): p. 4111-4119.
42. Loock, H.-P. and P.D. Wentzell, *Detection limits of chemical sensors: Applications and misapplications*. Sensors and Actuators B: Chemical, 2012. **173**(0): p. 157-163.